REVIEW

Check for updates

Recent progress on carbon materials for emerging zinc-ion hybrid capacitors

Lai Yu,† Jie Li,† Nazir Ahmad, Xiaoyue He, Guanglin Wan, Rong Liu, Xinyi Ma, Jiacheng Liang, Zixuan Jiang and Genqiang Zhang [ID] *

Zinc-ion hybrid capacitors (ZHCs) have gained increasing attention due to their numerous advantages such as cost-effectiveness, environmental friendliness, improved safety, high energy/power densities, and long-term cycling stability. However, despite these benefits, the development of ZHCs is still in its early stages with several challenges. Carbon materials have emerged as promising cathode candidates for application in ZHCs due to their low cost, abundance, diverse structures, and good electrical conductivity. In this review, we systematically summarize the research progress on carbon materials and the electrolytes for ZHCs, including activated carbon, graphene, porous carbon, and heteroatom-doped carbon materials. The synthetic methods, morphology characterization, electrochemical performance, and energy storage mechanisms for zinc-ion storage based on various types of carbon cathodes are comparatively discussed. Finally, the current challenges and prospects of carbon materials in zinc-ion storage systems are proposed. This review provides a comprehensive understanding of the research on carbon materials, which will be beneficial for the practical application of ZHC devices with high performance.

1. Introduction

The rapid consumption of fossil fuel resources has accelerated the development of sustainable and renewable energy resources to reduce environmental pollution and ease the looming energy crisis.[1,2] Efficient electrical energy storage systems are indispensable for storing intermittent renewable energy.[3] Among the various energy storage technologies, batteries and supercapacitors (SCs) are regarded as the two leading electrochemical energy-storage technologies.[4] Lithium-ion batteries (LIBs) have been used in various energy storage systems such as portable electronic devices and electric vehicles due to their high energy density and working voltage since their early commercialization in the 1990s.[5,6] However, LIBs still suffer from unsatisfactory cycle life and poor power output owing to their sluggish electron and ion transport.[7] In contrast, supercapacitors (SCs) have received widespread attention due to their high power density (>10 kW kg^{-1}) and long cycling lifespan (>100 000 cycles); however, their energy density is severely restricted (typically 5–10 W h kg^{-1}).[8] Hybrid ion capacitors that combine the advantages of both batteries and SCs using battery-type and capacitor-type electrodes to overcome these limitations, have been developed.[9] Although lithium-ion hybrid capacitors (LIHCs) have been extensively researched, their utilization can be improved due to issues such as the uneven

distribution of lithium resources, high cost, and the use of explosive and volatile organic electrolytes.[10] Therefore, hybrid capacitors based on multivalent cations, including Zn^{2+}, Mg^{2+}, Ca^{2+}, and Al^{3+}, have emerged as promising alternatives. These novel energy storage systems have attracted significant attention due to the abundance of these cations and their ability to carry more electrons per ion.[11,12] Fig. 1a shows the ionic radius, standard reduction potential, theoretical specific capacity, volumetric capacity, and metal cost of different metal electrodes.[13,14] Among the promising candidates, zinc-ion hybrid capacitors (ZHCs) show attractive priority given that zinc possesses a high theoretical capacity (820 mA h g^{-1} or 5855 mA h cm^{-3}) and low redox potential (−0.76 V vs. SHE, standard hydrogen electrode), as well as low cost, environmental friendliness and high safety of electrolytes.[16–21] Fig. 1b shows a comparison of the energy and power density diagrams of ZHCs with other usual energy storage systems.[15] Regarding energy and power densities, significant differences can be seen between batteries and SCs, while the assembled ZHCs can address the associated issues. As early as 2016, Wang *et al.*[22] reported a ZHC consisting of a zinc anode and oxidized carbon nanotube cathode in an aqueous ZnSO₄ electrolyte. The assembled ZHC device demonstrated a specific capacitance of 53 F g^{-1} and a stable cycling performance up to 5000 cycles. In 2018, Tang *et al.*[23] initially proved that a ZHC directly using Zn foil as both the anode and current collector and bio-carbon derived porous material as the cathode exhibited a superior electrochemical performance. Since then, the investigations on ZHCs have shown a rapidly growing trend (Fig. 1c), although the development of ZHCs is still in its infancy. Various cathode

Hefei National Laboratory for Physical Sciences at the Microscale, CAS Key Laboratory of Materials for Energy Conversion, Department of Materials Science and Engineering, University of Science and Technology of China, Hefei, Anhui 230026, China. E-mail: gqzhangmse@ustc.edu.cn

† Co-authors.

9400 | *J. Mater. Chem. A*, 2024, **12**, 9400–9420

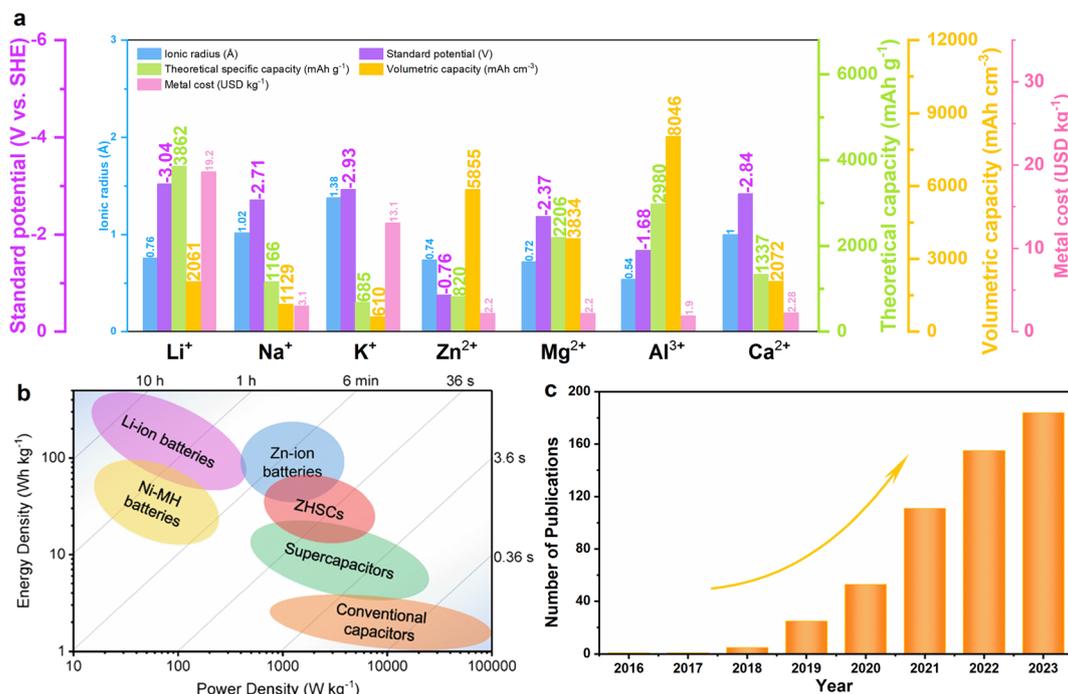This journal is © The Royal Society of Chemistry 2024

Fig. 1 (a) Ionic radius, standard reduction potential, theoretical specific capacity, volumetric capacity, and metal cost of different metals. (b) Energy density and power density profiles of ZHCs and other energy storage devices. Copyright 2020, Wiley–VCH.[15] (c) Number of publications on ZHCs according to Web of Science (from 2016 to December 2023).

materials, including carbon materials, transition metal oxides, MXene, and phosphorene, have attracted growing research interest.[24–29] For example, in 2019, the amorphous $RuO_2 \cdot H_2O$ cathode material was employed for the first time, achieving the outstanding electrochemical performance of Zn^{2+} storage based on a pseudocapacitive storage mechanism. This cathode exhibited a high specific capacity of 122 mA h g^{-1} at 0.1 A g^{-1} and a maximum energy density of 119 W h kg^{-1}, as well as an ultralong cycle life exceeding 10 000 cycles.[29] In addition, the electrolyte (such as $ZnSO_4$, $Zn(CF_3SO_3)_2$, and $ZnCl_2$), as another basic component, also plays an important role in the electrochemical performance of ZHCs.[30,31] For example, Chen et al.[32] reported the use of a ZHC with activated carbon (AC) as the negative electrode and 2 M $ZnCl_2$ as the electrolyte, which displayed a high capacitance of 229.4 F g^{-1} and superior rate capability, suggesting that the Cl^- in the aqueous $ZnCl_2$ electrolyte could improve the energy storage capacity of porous carbon materials. Also, some works investigated the structure change and efficient utilization of Zn metal anodes due to the dendrite growth and corrosion during cycling. Xia et al.[33] demonstrated that a microporous Zn-based metal–organic framework (MOF) as a host matrix for electrodeposited Zn showed high efficiency and dendrite-free characteristic. Then, the composite was coupled with a commercial AC cathode to form a hybrid supercapacitor, which exhibited outstanding cyclic stability up to 20 000 cycles. These achievements promote the development of ZHCs, which can guide further investigations for next-generation energy storage devices.

Among the various cathode materials, carbon materials have recently garnered extraordinary focus due to their abundant resources, high electronic conductivity, super-specific surface area and tunable pore structures.[34–36] Currently, carbon materials with different morphologies and structures are employed as cathode materials in ZHCs, such as AC and porous carbon, demonstrating superior electrochemical performances. The carbon cathode can store electrical energy based on reversible ion adsorption/desorption, while the physical and chemical properties of carbon materials can determine the electrochemical performance of ZHCs.[15] However, despite their significant merits, there are still some challenges for carbon cathodes to acquire a high performance because of the kinetic imbalance between the carbon-based cathode and Zn anode and the lack of understanding of the charge storage mechanism. Therefore, there is still much room for improvement to get high-performance ZHCs by designing and optimizing carbon materials. Hence, in this review, we systematically summarize the application and research progress of carbon materials, including AC, graphene, porous carbon, and heteroatom-doped carbon materials in ZHC devices (Fig. 2). The synthesis, structure, electrochemical performance, and energy storage mechanisms of carbon materials are investigated systematically. Finally, based on the in-depth understanding of the achievements of carbon cathodes, the existing challenges and perspectives of carbon materials in zinc ion storage systems are proposed.

2. Supercapacitors and hybrid capacitors

2.1 Principle of energy storage in supercapacitors

The metal ion battery is a typical "rocking chair" battery (Fig. 3a), in which the reversible M^{n+} insertion/extraction in the
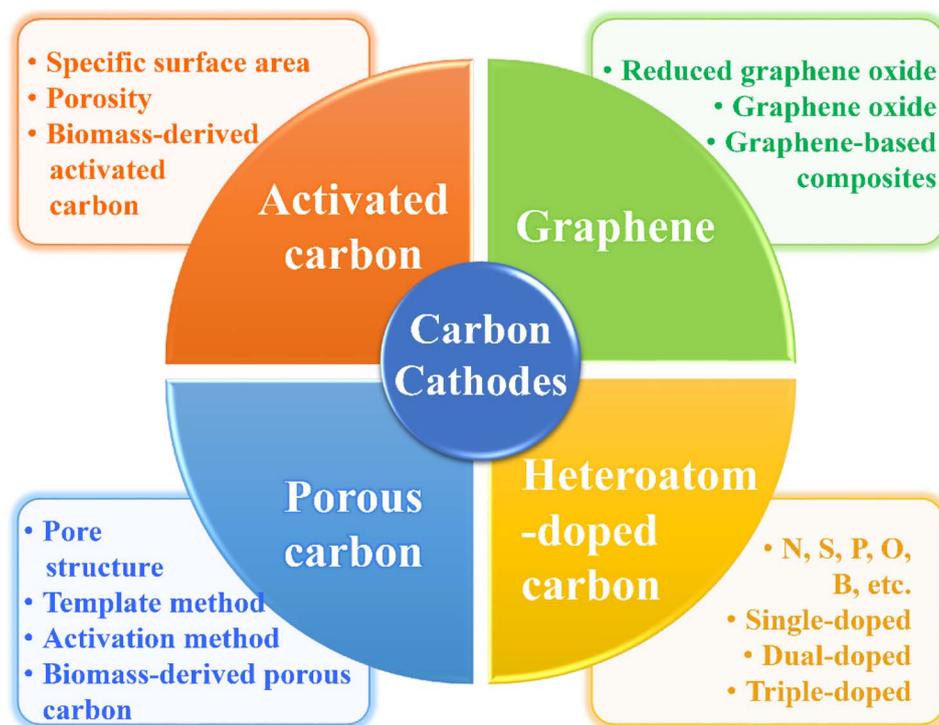
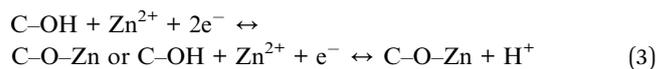Fig. 2 Summary of carbon cathode materials discussed in ZHCs.

host materials is the main charge storage mechanism.[37] Alternatively, SCs are mainly composed of electrodes and electrolytes. Normally, SCs can be divided into two categories based on their energy storage mechanisms (Fig. 3b), *i.e.*, electrochemical double-layer capacitors (EDLCs, physical adsorption/desorption of electrolyte ions on the surface of electrodes) and pseudocapacitors (fast and reversible surface redox reactions).[38,39] SCs exhibit outstanding power density and long cycling stability. As an EDLC material, AC is usually employed as the working medium due to its high surface area and porous structure, which can store much more electricity than other materials. Meanwhile, the cyclic voltammogram (CV) of EDLC-based materials is almost rectangular, and their corresponding charge–discharge curve is linear with a constant slope during charge/discharge processes.[40] Alternatively, pseudocapacitive electrode materials can store charge *via* the faradaic charge transfer process, for instance, RuO_2 and MnO_2.[41,42] There are three types of faradaic mechanisms including underpotential deposition, redox pseudocapacitance, and intercalation pseudocapacitance,[4,43,44] as follows: (1) underpotential deposition happens when metal ions form an absorbed monolayer on the surface of the metal (*e.g.*, Pt and Ru) above their reversible redox potential; (2) redox pseudocapacitance happens on the surface or near-surface of electrodes due to a rapid, reversible faradaic redox reaction and (3) intercalation pseudocapacitance occurs when ion intercalation occurs in the tunnels or layers of the redox-active material (*e.g.*, Nb_2O_5) without a crystallographic phase change. Besides, pseudocapacitive electrodes show a pseudo-rectangular CV shape and an analogous triangular-shaped galvanostatic charge–discharge curve.

2.2 The energy storage mechanism of zinc ion hybrid capacitors

Most ZHCs are assembled using a capacitor-type cathode (such as carbon cathode materials) and a Zn metal (or a modified metal Zn) anode with mild Zn salt solutions such as $ZnSO_4$ electrolyte (Fig. 3c).[45] In the case of the anode, the energy storage mechanism is the plating/stripping reaction of Zn to provide a high energy density, which can be described as follows:[46]

$$Zn \leftrightarrow Zn^{2+} + 2e^- \quad (1)$$
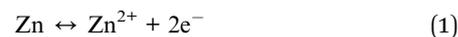
Regarding the capacitor-type carbon material cathode, the capacitance is mainly contributed from the EDLC storage with reversible ion adsorption/desorption and pseudocapacitance by chemical adsorption of Zn ions at/near the surface of the carbon electrode, especially those involving oxygen functional groups or doped heteroatoms to gain a superpower density, which is expressed as follows:[17,47]

$$C + X^- \leftrightarrow C//X^-; \ C + Y^+ \leftrightarrow C//Y^+ \ (X: anions, Y: cations) \quad (2)$$

$$C–OH + Zn^{2+} + 2e^- \leftrightarrow$$
$$C–O–Zn \ or \ C–OH + Zn^{2+} + e^- \leftrightarrow C–O–Zn + H^+ \quad (3)$$

$$COOH + Zn^{2+} + 2e^- \leftrightarrow COO–Zn + H^+ \quad (4)$$

However, there are some side reactions in aqueous electrolytes besides the primary reactions on the electrodes, where the OH^- ions produced from the hydrogen evolution reaction can

9402 | *J. Mater. Chem. A*, 2024, **12**, 9400–9420

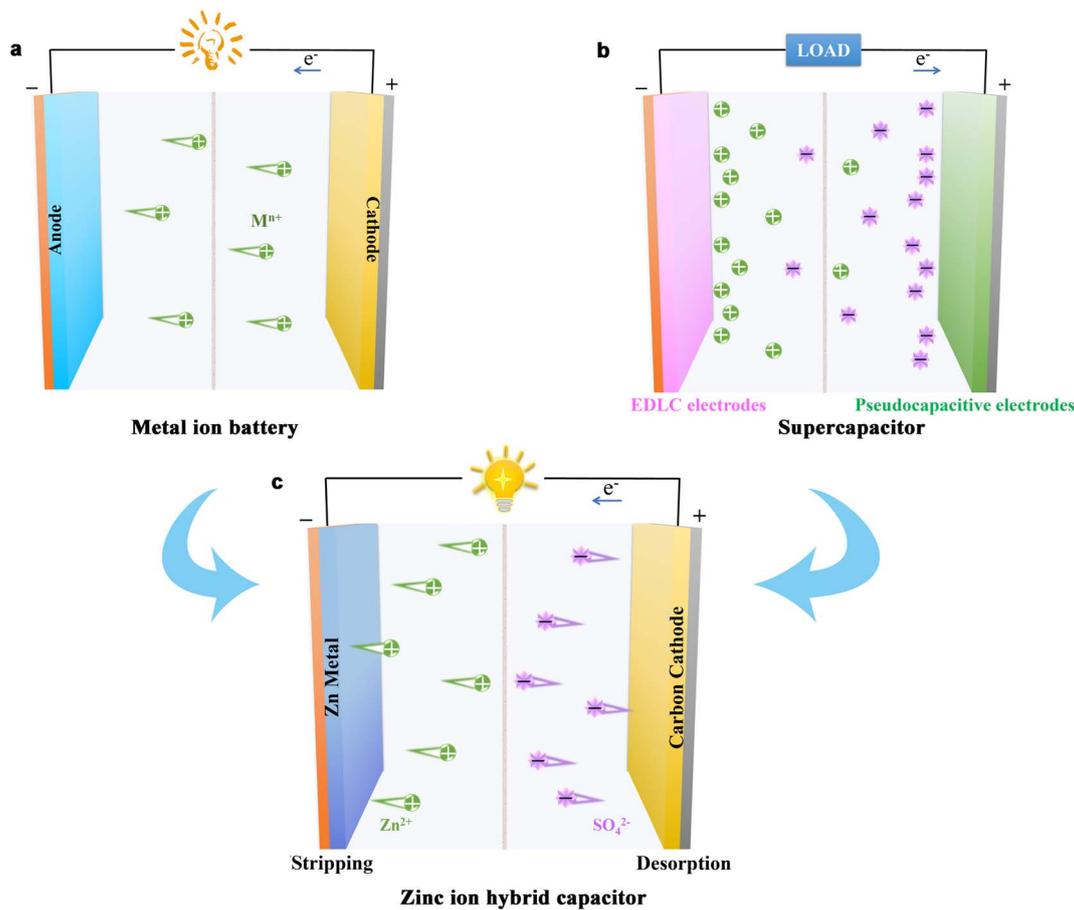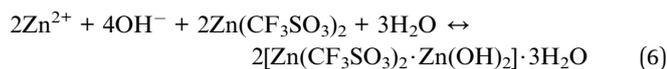This journal is © The Royal Society of Chemistry 2024

Fig. 3 Schematic of the chemical reactions in different types of energy storage devices: (a) metal ion battery, (b) supercapacitor, and (c) zinc ion hybrid capacitor.

react with Zn^{2+} in the aqueous electrolyte (such as $ZnSO_4$ and $Zn(CF_3SO_3)_2$). The process can be presented as follows:[48,49]

$$4Zn^{2+} + 6OH^- + SO_4^{2-} + 5H_2O \leftrightarrow Zn_4SO_4(OH)_6 \cdot 5H_2O \quad (5)$$

$$2Zn^{2+} + 4OH^- + 2Zn(CF_3SO_3)_2 + 3H_2O \leftrightarrow 2[Zn(CF_3SO_3)_2 \cdot Zn(OH)_2] \cdot 3H_2O \quad (6)$$

The formation/decomposition of $Zn_4SO_4(OH)_6 \cdot 5H_2O/$ $[Zn(CF_3SO_3)_2 \cdot Zn(OH)_2] \cdot 3H_2O$ is reversible on the cathode electrodes during the charge/discharge process. The researchers proposed that side reactions can lead to the loss of capacity, while some workers think that the reactions may contribute slightly to the whole energy storage. Therefore, the storage mechanism still needs to be investigated in depth.

3. Research progress of carbon materials

Carbon materials exhibit the advantages of large specific surface area (SSA), high electronic conductivity, and fast charge transport, representing a promising candidate in various energy storage systems.[50,51] They not only play an essential role in commercial metal ion batteries, such as LIBs and sodium-ion

batteries (SIBs), but also can be used in emerging energy storage devices such as ZHCs.[52,53] In this section, the latest advances in AC, graphene, porous carbon, and heteroatom-doped carbon materials as cathodes in ZHCs will be introduced, especially in terms of their synthesis, structure, electrochemical performance, and energy storage mechanisms.

3.1 Activated carbon

AC is mainly composed of local, aromatic configuration layers of carbon atoms, possessing a high surface area and good spatial structure, which has been widely used in batteries and supercapacitors due to its unique characteristics.[54–56] In recent years, AC has been applied in the emerging ZHCs since its application as a cathode by the Tang group (Fig. 4a).[23] AC was prepared from coconut shells and KOH activation, resulting in a high surface area (3384 $m^2 g^{-1}$), wide operation window (0–1.8 V), and nontoxicity. The fabricated ZHCs with AC cathode and zinc anode in 1 M $Zn(CF_3SO_3)_2$ electrolyte achieved a high discharge capacitance of 170 F g^{-1} at 0.1 A g^{-1}, high energy density of 52.7 W h kg^{-1} at 1725 W kg^{-1}, and ultralong cycle life of 20 000 cycles with 91% capacitance retention at a current density of 2 A g^{-1} (Fig. 4b). Meanwhile, Kang et al.[46] designed a ZHC device using commercial AC, Zn metal, and 2 M $ZnSO_4$

This journal is © The Royal Society of Chemistry 2024

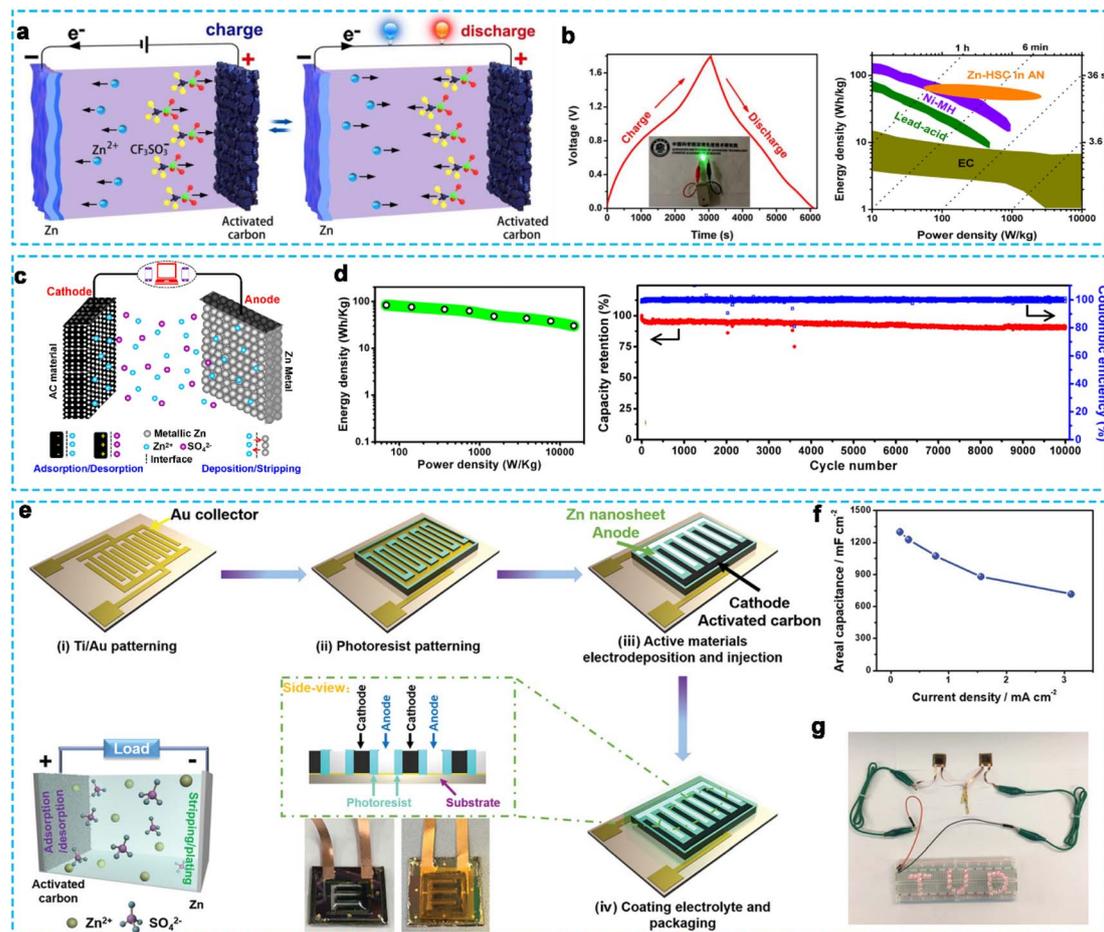J. Mater. Chem. A, 2024, **12**, 9400–9420 | **9403**

Fig. 4 (a) Schematic illustration of working mechanism and (b) electrochemical performance of the ZHCs based on AC cathode.[23] Copyright 2018, Elsevier. (c) Schematic of AC//ZnSO$_4$ (aq.)//Zn energy storage system and (d) corresponding electrochemical performance.[46] Copyright 2018, Elsevier. (e) Schematic of the fabrication process of Zn-ion hybrid micro-supercapacitors, (f) rate capability, and (g) two connected Zn-ion hybrid micro-supercapacitors lighting up a red LED.[61] Copyright 2019, Wiley-VCH.

aqueous solution as the cathode, anode, and electrolyte, respectively, which exhibited a high energy density of 84 W h kg^{-1} at 69 W kg^{-1}, superpower output of 14.9 kW kg^{-1} at 30 W h kg^{-1}, and excellent cycling stability with 91% capacity retention for 10 000 cycles at 1 A g^{-1} (Fig. 4c and d). However, the traditional AC suffers from low capacity and poor rate performance due to its poor wettability, dominant micropore porosity, poor ionic diffusion and transport ability. Thus, to further solve these problems, Zhou et al.[57] proposed a hierarchical porous AC (HPAC) via an in situ two-step activation procedure during the carbonization process of asphalt with KOH, showing a high SSA of 3525 m^2 g^{-1} and a large mesoporous volume. Subsequently, the advanced ZHC device was assembled with an HPAC cathode and Zn anode in 3 M Zn(CF$_3$SO$_3$)$_2$ aqueous electrolyte, which delivered a high specific capacity of 231 mA h g^{-1} at 0.5 A g^{-1} and excellent rate performance with a retained capacity of 119 mA h g^{-1} at 20 A g^{-1} (77.5 W h kg^{-1} at 11.4 kW kg^{-1}) in the voltage range of 0.01–1.8 V, and an ultra-long lifespan with a capacity retention of 70% after 18 000 cycles at 10 A g^{-1}, which was better than that of commercial AC. In addition, Geon-Hyoung An[58] synthesized

AC with an engineered surface and mesoporous structure (MSAC) using a dehydrogenation process of polyvinylpyrrolidone for ZHCs. The mesoporous-structured AC showed a high SSA of 2527 m^2 g^{-1} and a high pore volume of 2.7 cm^3 g^{-1}, which could shorten the ionic diffusion pathway during ultrafast cycling. The optimized ZHC based on the MSAC cathode displayed a high capacity of 176 mA h g^{-1} at 0.5 A g^{-1}, outstanding rate capability of 72 mA h g^{-1} at 10 A g^{-1}, maximum energy density of 188 W h kg^{-1} at 533 W kg^{-1}, and maximum power density of 10 666 W kg^{-1} at 77 W h kg^{-1}, accompanied with impressive cycle stability with 78% capacity retention at 10 A g^{-1}. More importantly, to further realize the practical application of ZHCs, some workers have started to design multifunctional zinc-ion energy storage devices (such as flexible zinc-ion hybrid capacitors and microdevices).[59] For example, Xu et al.[60] designed a flexible solid-state ZHC employing commercial AC as the cathode material and Zn foil as the anode electrode. A zwitterionic natural polymer hydrogel with ZnSO$_4$ electrolyte acted as the solid-state gel electrolyte, exhibiting excellent mechanical strength and flexibility. Therefore, the flexible ZHC device showed a high energy density of

9404 | J. Mater. Chem. A, 2024, 12, 9400–9420

This journal is © The Royal Society of Chemistry 2024

286.6 W h kg^{-1} at the power density of 220 W kg^{-1} in a wide voltage window and good cycle stability with a capacity retention of 95.4% after 2000 cycles at 2 A g^{-1}. The device exhibited favorable flexibility and electrochemical stability at different bending angles (0° to 180°). Notably, the carbon cathode also played a pivotal role in the electrochemical performance, besides the key component of the gel electrolyte. High porosity is an efficient way to improve the electrochemical properties of carbon materials, such as specific capacity, rate performance, and cycling ability. Alternatively, Feng et al.[61] reported the preparation of a new-type Zn-ion hybrid micro-supercapacitor by employing AC as the cathode and electrodeposited Zn nanosheets as the anode in a ZnSO$_4$-based electrolyte (Fig. 4e). As shown in Fig. 4f, the microdevice exhibited a high areal capacitance of 1297 mF cm^{-2} at 0.16 mA cm^{-2} (259.4 F g^{-1} at a current density of 0.05 A g^{-1}), landmark areal energy density of 115.4 μW h cm^{-2} at 0.16 mW cm^{-2}, and remarkable cycling stability without noticeable decay after 10 000 cycles. Importantly, the two serially connected Zn-ion hybrid micro-supercapacitors could light red light-emitting diodes (LEDs), indicating their potential for practical application (Fig. 4g). Thus, it can be seen that an AC cathode with high SSA and high pore volume can generate more active sites for ion adsorption and facilitate ion transfer, enhancing the electrochemical performance of ZHCs.

Biomass-derived AC is a potential carbon material for energy storage devices due to its unique physical/chemical properties, abundant functionality, and economic value, which is prepared by physical, chemical, physiochemical, and microwave-assisted activation.[62,63] He and co-workers[64] prepared AC derived from corncob (denoted as ACC), which had a high SSA of 2619 m^2 g^{-1}

with a hierarchical porous structure by tuning the parameters in a calcination–activation process (Fig. 5a–c). The assembled ZHC exhibited a high energy density of 94 W h kg^{-1} at 68 W kg^{-1} and superior cycling stability with 98.2% capacitance retention after 10 000 cycles at 5 A g^{-1}. Recently, Zhou and co-researchers[65] synthesized coconut shell-activated carbon (CSAC) via a steam activation method (Fig. 5d). The SSA of CSAC was 1260 m^2 g^{-1} with a pore volume of 1.8 cm^3 g^{-1}, and its porosity was concentrated at around 1.03 nm (Fig. 5e), which could accelerate the kinetics of the electrolyte ions and provided sufficient active sites for charge storage. Consequently, a robust, flexible quasi-solid-state ZHC device (Fig. 5f) was fabricated using CSAC as the cathode and cross-linked poly(vinyl alcohol)/montmorillonite/Zn(ClO$_4$)$_2$ as the gel electrolyte, which showed high energy/power densities (49.1 W h kg^{-1}/6.5 kW kg^{-1} at −20 °C and 138.6 W h kg^{-1}/18 kW kg^{-1} at 60 °C), and excellent cycling stability in a wide temperature range from −50 °C to 80 °C (such as 99% capacity retention at 25 °C and 98% capacity retention at −20 °C after 10 000 cycles at 5 A g^{-1}, respectively). Likewise, the electrochemical performance of the quasi-solid-state ZHC device remained virtually unchanged at different angles from 0° to 120°, demonstrating its admirable mechanical flexibility. According to the above discussion, the use of AC with high SSA and tailored porosity as the cathode electrode is necessary for ZHCs (or multifunctional zinc ion energy storage devices) to achieve high energy/power density and superior cycling stability.

3.2 Graphene

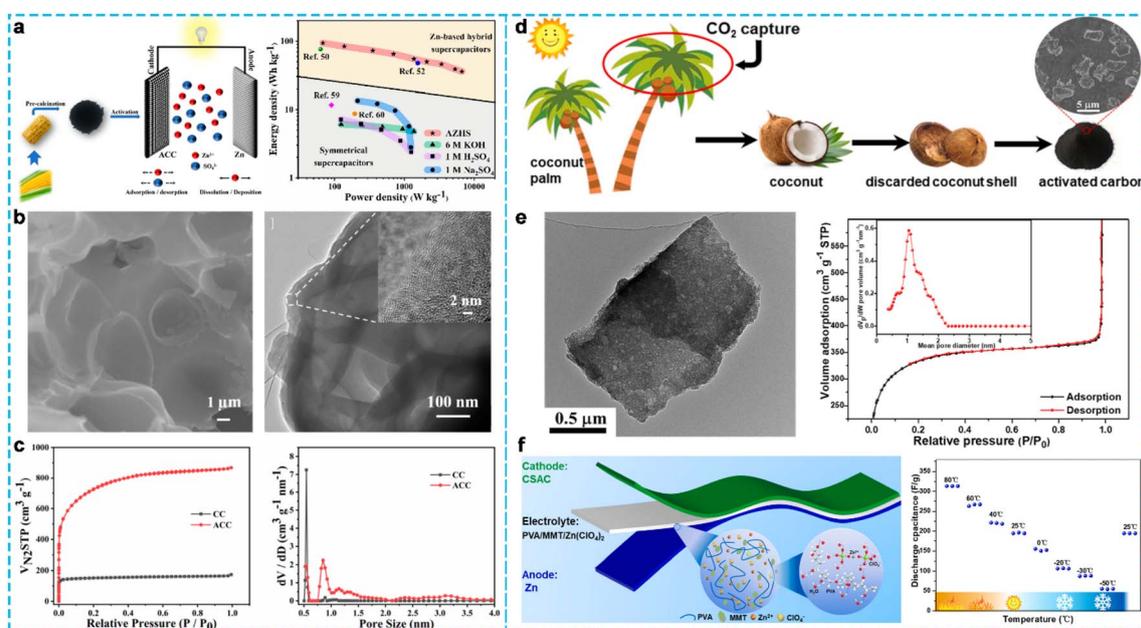Graphene is a two-dimensional (2D) nanomaterial composed of layers of carbon atoms in a hexagonal honeycomb lattice.[66] In

Fig. 5 (a) Schematic illustration for the preparation of ACC, (b) the SEM and TEM images of ACC, (c) N$_2$ adsorption–desorption isotherms, and pore size distribution of ACC.[64] Copyright 2019, American Chemical Society. (d) Schematic illustration of the coconut cycle of coconut, coconut shell, and biochar and (e) the structural study of CSAC. (f) The electrochemical performance of quasi-solid-state ZHC device.[65] Copyright 2021, Elsevier.

This journal is © The Royal Society of Chemistry 2024

J. Mater. Chem. A, 2024, **12**, 9400–9420 | **9405**

recent years, graphene has attracted significant attention in various fields due to its remarkable physicochemical properties, such as high theoretical surface area (2630 m^2 g^{-1}), excellent electronic conductivity (5000 S m^{-1}), large intrinsic electron mobility (200 000 cm^2 V^{-1} s^{-1}) and high porosity.[67] In addition, the derivatives of graphene, such as graphene oxide (GO) and reduced graphene oxide (rGO), containing oxygenated groups and defects, can be ideal cathode candidates for ZHCs. Yan et al.[68] constructed a dense three-dimensional (3D) graphene (DGH) with an SSA of 208.29 m^2 g^{-1} and high density of 1.50 g cm^{-3}, facilitating the fast transfer of ions/electrons and ensuring sufficient charge storage sites. The ZHC device using the prepared DGH as a cathode exhibited an extremely high volumetric energy density of 118.42 W h L^{-1}, superb power density of 24.00 kW L^{-1}, and ultralong cycle stability of 30 000 cycles with 80% capacity retention at a high current density of 10 A g^{-1}. Jia's group[69] prepared free-standing graphene hydrogel films with a controlled structure by controlling the swelling of the graphene oxide film (Fig. 6a). In contrast, the swelling degree of GO films in water was adjusted by changing the acting force among adjacent GO sheets, such as van der Waals, hydrogen bonding, and electrostatic repulsion. The assembled ZHC device with graphene hydrogel film cathode in 2 M ZnSO$_4$ electrolyte showed a large capacity of 99.3 mA h g^{-1} at 0.2 A g^{-1}, high energy density of 72.6 W h kg^{-1}, and excellent capacity retention property of 90% after 10 000 cycles (Fig. 6b). The high performance of the device was ascribed to its rich pore structure, which could provide ion-buffering reservoirs and ion transport channels. Zhang's group[70] developed porous carbon derived from chemically activated graphene (aMEGO) with an

SSA of 2957 m^2 g^{-1} and uniform pore size distribution. When assembled with a Zn anode to form a ZHC in aqueous 3 M Zn(CF$_3$SO$_3$)$_2$ electrolyte, it demonstrated a high energy density of 106.3 W h kg^{-1} and maximum power density of 31.4 kW kg^{-1} in a wide operating voltage of 0–1.9 V. Moreover, the device exhibited an ultralong cycling life of up to 80 000 cycles with 93% capacity retention at a high current density of 8 A g^{-1}.

Oxygen-bonded and defective rGO was synthesized via a modified Hummers' method, which could be employed as an active material for ZHCs.[71] The device exhibited a specific capacity of 200.4 F g^{-1} at 0.1 A g^{-1} and a capacity retention of 92.06% after 10 000 cycles at 5 A g^{-1}. When the system was exposed to air, a higher specific capacity (370.8 F g^{-1} at 0.1 A g^{-1}) and high energy density (100.9 W h kg^{-1} at 70 W kg^{-1}) could be obtained, as well as superior cycling stability with 94.5% capacitance retention after 10 000 cycles. More importantly, apart from the physical adsorption/desorption of ions on the surface of graphene, oxygen-containing functional groups and defects can be generated in the oxygen reduction reaction and provide more active sites for the electrochemical adsorption/desorption of Zn^{2+}, providing extra capacitance to enhance the performance of ZHCs. However, the influence of oxygen substituents of the carbon cathode on the energy storage behavior of ZHCs is vague. Therefore, Sun et al.[72] studied the impact of the surface oxygen substituents on the pseudocapacitance contribution and chemical adsorption of Zn ions (Fig. 6c). They chemically synthesized rGO with oxygen functional groups using a series of reductants and varying experimental conditions, which could provide redox-active pseudocapacitance and strengthen the Zn ion adsorption/
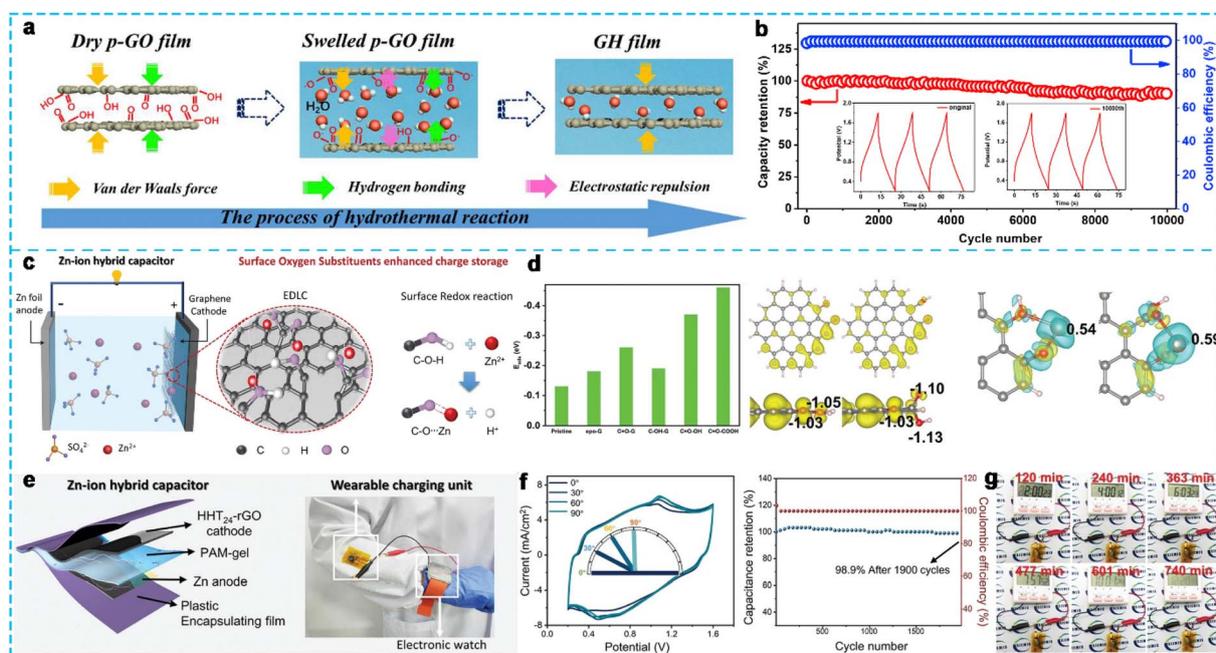

Fig. 6 (a) Schematic diagram of the interlayer space evolution of graphene films during the hydrothermal reaction and (b) cycling performance of the ZHC device at a high current density of 15 A g^{-1}.[69] Copyright 2020, Elsevier. (c) Schematic of the configuration and working mechanism of ZHCs with surface oxygen functional groups and (d) DFT calculations. (e) Schematic diagram of the as-assembled quasi-solid-state ZHC, (f) electrical performance, and (g) photograph of the device-powered timer at different discharge times.[72] Copyright 2020, Wiley-VCH.

9406 | J. Mater. Chem. A, 2024, 12, 9400–9420

This journal is © The Royal Society of Chemistry 2024

desorption to enhance the overall ZHCs electrochemical performance. Moreover, the researchers used density functional theory (DFT) to confirm that the carboxyl and carbonyl groups could reduce the chemical adsorption barrier of Zn^{2+} (Fig. 6d), boost the surface wettability, and extend the stable working potential, thus enhancing the Zn-ion chemical adsorption ability and electrochemical charge storage. Consequently, the ZHC-based rGO cathode synthesized through hydrogen peroxide-assisted hydrothermal reduction exhibited a high specific capacitance of 277 F g^{-1} and capacitance retention of 97.8% after 20 000 cycles even at a relatively low current density of 2.5 A g^{-1} in 1 M $ZnSO_4$ electrolyte. Alternatively, a quasi-solid-state ZHC with an rGO cathode and a polyacrylamide gel electrolyte was assembled to investigate its possible application (Fig. 6e). The ZHC device, with great flexibility, could deliver an outstanding areal capacitance of 1257 mF cm^{-2}, high areal energy density of 342 μW h cm^{-2}, and power density of 880 mW cm^{-2}, as well as a great capacity retention of 98.9% after 1900 cycles (Fig. 6f). An electric timer could be powered for more than 12 h by two quasi-solid-state ZHCs connected in series (Fig. 6g), demonstrating that the quasi-solid-state ZHC device is a promising flexible power source. As can be seen, the rGO-based ZHCs exhibited a superior performance due to the additional pseudocapacitance provided by the oxygen-containing functional groups.

The agglomeration effect of multilayer graphene sheets causes an unsatisfactory capacitance in graphene electrodes. Thus, to solve this problem, Xu et al.[73] designed a p-phenylenediamine (PPD) organic molecule-functionalized rGO film via simple hydrothermal reduction using PPD as a reducing and functional agent. Benefiting from the three-dimensional (3D) structure of the covalently grafted PPD, increasing the wettability and enhancing the electroconductivity of the RGO film, the fabricated ZHCs utilizing the optimized rGO@PPD (6 : 7, mass ratio) film cathode and Zn anode displayed a high areal capacitance (3012.5 mF cm^{-2} at 1 mA cm^{-2}), sufficient energy density (1.1 mW h cm^{-2} at a power density of 0.8 mW cm^{-2}) in aqueous 1.0 M $Zn(CH_3COO)_2$ electrolyte, and retention of the initial areal capacitance after 4000 cycles at 7 mA cm^{-2}. Prasit Pattananuwat et al.[74] combined the conducting polymer polypyrrole (PPy) with nitrogen-doped graphene (N-rGO) via in situ polymerization for ZHCs. The synthetic PPy nanoparticles embedded on N-rGO showed a 3D network structure with a high SSA of 89.82 m^2 g^{-1} and large mesopore structure, facilitating ion/charge transportation and affording rapid transport channels for Zn ion adsorption/desorption. The constructed ZHCs using zinc foil as the anode and N-rGO/PPy as the cathode with 0.2 M $ZnSO_4$ exhibited a high specific capacity (145.32 mA h g^{-1} at 0.1 A g^{-1} in the potential range of 0–1.6 V), remarkable energy density (232.50 W h kg^{-1} at 160 W kg^{-1}), and excellent cycling stability of 85% retention up to 10 000 cycles at 7.0 A g^{-1}. In addition, the energy storage mechanism of the N-rGO/PPy cathode was the adsorption/desorption of Zn^{2+} ions on the cathode surface and the intercalation/deintercalated of Zn^{2+} ions in the PPy structure via a faradaic reaction, enhancing the storage capability of the N-rGO/PPy cathode-based ZHCs. Likewise, Jiang et al.[75] fabricated a ZHC device using electrochemically exfoliated graphene/polyaniline (EG/PANI) as the cathode and porous organic polymer–tetra(4-aminophenyl) porphyrin–1,4,5,8-naphthalenetetracarboxylic dianhydride (POP–TAPP–NTCA) as the anode in 2 M $ZnSO_4$ aqueous electrolyte, which exhibited a specific capacitance of 172 F g^{-1}, maximum energy density of 48 W h kg^{-1} and capacitance retention of 90% after 1100 cycles at a low current density of 0.3 A g^{-1}. Also, Yang et al.[76] reported the fabrication of a ZHC device using a polypyrrole/electrochemical graphene oxide (PPy/EGO) composite cathode in aqueous 1 M $ZnCl_2$ electrolyte, exhibiting a great energy density of 117.7 W h kg^{-1} at 0.34 kW kg^{-1}, high power density of 12.4 kW kg^{-1} at 72.1 W h kg^{-1}, and long-term cycling stability with 81% capacitance retention after 5000 cycles. Interestingly, they thought the PPy/EGO cathode charge storage mechanism in ZHCs mainly involved fast monovalent anion (e.g., Cl^- and Br^-) insertion/de-insertion into/from PPy instead of Zn^{2+} ion insertion/de-insertion. Therefore, compounding polymers with graphene is an effective way to improve the specific capacitance of ZHCs. However, some issues still need to be overcome, such as the high cost and complicated operation of the method for the synthesis of graphene-based composites. Furthermore, understanding the charge storage mechanism of graphene-based composite systems needs further research.

3.3 Porous carbon

Porous carbon is the most widely applied material in ZHCs because of its high SSA and pore volume, tunable porous structures, and unique morphologies, which can be synthesized by activation and template methods, such as soft templating, hard templating, and self-templating.[15,77] Besides, the pores can be divided into microporous (<2 nm), mesoporous (2–50 nm), macroporous (>50 nm), and hierarchical porous (micro–meso–macroporous) according to their size.[78] Notably, porous carbon differs from the above-mentioned activated carbon cathode in various aspects, including composition, preparation process and physicochemical properties. Porous carbon can deliver better ion storage ability because of its tuned surface characteristics, hierarchical porous structure, and tailored architecture with large pore volume.[79] Chen et al. synthesized hollow carbon spheres (HCSs) via the carbonization of polyaniline-co-polypyrrole hollow spheres as a soft template (Fig. 7a).[80] The HCSs possessed a high SSA of 819.5 m^2 g^{-1} and mesoporous structure caused by the carbonization of the copolymers (Fig. 7b). Firstly, they reported the fabrication of a high-performance flexible solid-state ZHC using HCSs as the cathode and a polyacrylamide hydrogel as the electrolyte, delivering a high capacity of 86.8 mA h g^{-1} and a maximum energy density of 59.7 W h kg^{-1} at 447.8 W kg^{-1}. Especially, the device displayed excellent cycling stability with 98% capacity retention for up to 15 000 cycles at a low current density of 1.0 A g^{-1} (Fig. 7c). Subsequently, the Ci group[81] constructed ultrathin porous carbon nanosheets (Ca-900) via a facile in situ template method with calcium gluconate as the carbon source. Ca-900 exhibited hierarchically porous structures with an SSA of 955.08 m^2 g^{-1}, offering abundant channels and spaces for the
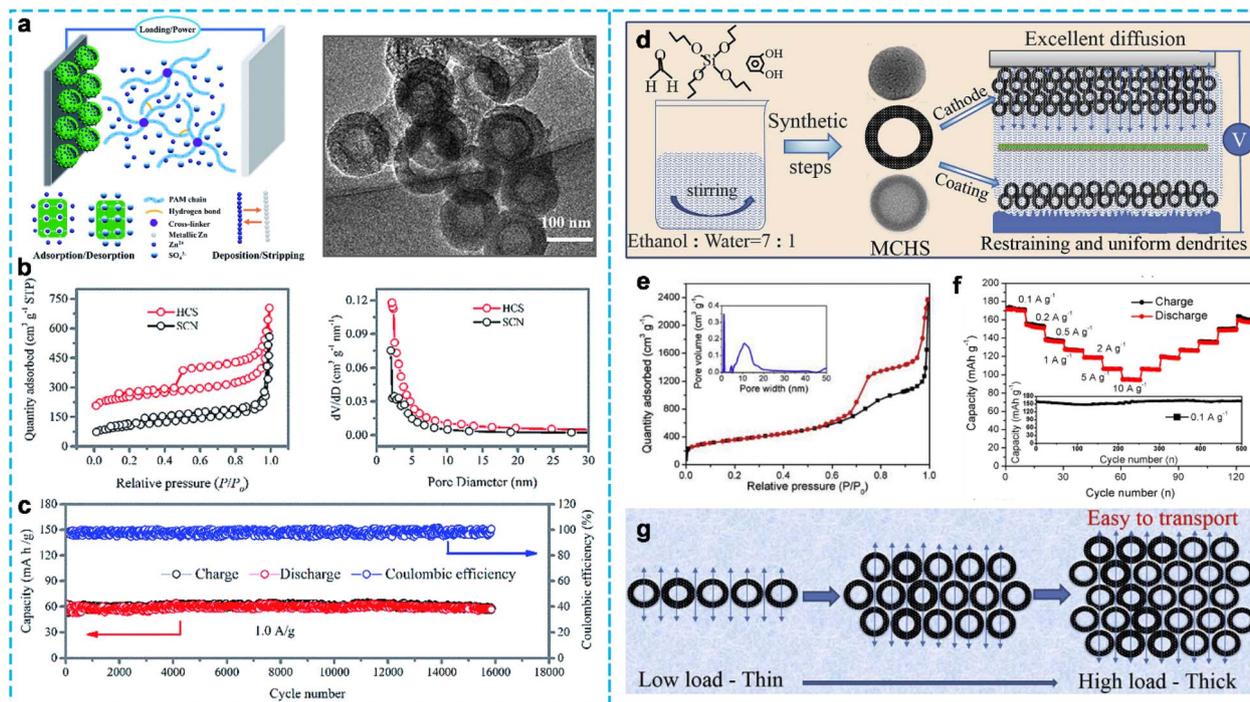
Fig. 7 (a) Schematic illustration of the working principle of the ZHCs and corresponding morphology of HCSs, (b) N$_2$ adsorption−desorption isotherms and pore diameter distributions of HCSs, and (c) cycle performance of the HCS cathode at 1.0 A g^{-1}.[80] Copyright 2019, The Royal Society of Chemistry. (d) Synthesis process and application of MCHSs, (e) N$_2$ sorption isotherms (inset is the pore size distribution), (f) rate performance, and (g) scheme of the ion transport processes in MCHSs with different mass loadings.[82] Copyright 2020, Elsevier.

diffusion of ions. As a result, the Ca-900 cathode-based ZHC obtained a high energy density of 75.22 W h kg^{-1} at 36.56 W kg^{-1} and cycling stability with ∼90% capacity retention after 4000 cycles at 1.0 A g^{-1}. However, they showed good cycling stability but poor specific capacity and rate performance. Hence, Liu *et al.*[82] fabricated mesoporous carbon hollow spheres (MCHSs) using a typical silica template with a high SSA of 1275 m^2 g^{-1} and pore volume of 1.73 cm^3 g^{-1} (Fig. 7d and e). The hierarchical micro–mesoporous structure was conducive to ion adsorption/desorption and transport, increasing the electric double-layer capacitance. The assembled ZHCs with MCHSs as the cathode and MCHS-coated Zn foil as the anode (Fig. 7f) achieved a high specific capacity (174.7 mA h g^{-1} at 0.1 A g^{-1}), good rate capability (96.9 mA h g^{-1} at 10 A g^{-1}), high energy density (129.3 W h kg^{-1} at 266.4 W kg^{-1}) and maximum power density (13.7 kW kg^{-1} at 36.8 W h kg^{-1}), which was higher than that of the AC cathode-based ZHC. Even at a high mass loading of 20 mg cm^{-2}, it exhibited a high gravimetric and ultrahigh areal capacitance, which was attributed to the short ion and charge transport path and good penetration provided by the interconnected porous of MCHSs (Fig. 7g). Similarly, Fan *et al.*[83] also designed an asymmetric hollow bowl-like carbon (HBC) material *via* an *in situ* hard-template approach (silica spheres). Benefitting from its abundant mesopores, high surface area of 791.5 m^2 g^{-1}, and open macropore network, the ZHC full device using the HBC cathode delivered a specific capacity of 95.4 mA h g^{-1} at 0.1 A g^{-1}. Also, it retained 43.6 mA h g^{-1} at a high current density of 20 A g^{-1}.

Another method is the activation method, among which chemical activation is the most common using activating agents such as KOH, K$_2$CO$_3$, and NaOH.[84] Wang *et al.*[85] prepared a new type of sharpened pencil-like nanoporous carbon (MPC-*x*, where *x* represents the ratio of KOH) by using a metal–organic framework (MIL-47) as the precursor combined with the chemical activation method (Fig. 8a–d). MPC-2 possessed a high SSA of 2125 m^2 g^{-1} and a large pore volume of 2.21 cm^3 g^{-1}, which facilitated the expansion of the active interface and promoted the ion transfer rate. The assembled ZHCs achieved a high energy density of 130.1 W h kg^{-1} at 180.3 W kg^{-1} and a large power density of 7.8 kW kg^{-1} at 59 W h kg^{-1} under a relatively wide operating voltage of 0–1.8 V, as well as excellent cycling stability over 10 000 cycles at 10 A g^{-1}. Likewise, Fan *et al.*[86] obtained porous honeycomb carbon (PPC) with a high SSA of 2926.4 m^2 g^{-1} by a pre-oxidation and KOH-activated process. Due to the interconnected structure of porous carbon, the Zn//PPC ZHCs displayed a high specific capacity of 238 mA h g^{-1} at 0.1 A g^{-1}, maximum energy density of 193.6 W h kg^{-1} at 76.6 W kg^{-1} and maximum power density of 3981 kW kg^{-1} at 109.5 W h kg^{-1}, together with a superior cycle life of up to 20 000 cycles with a capacity retention of 83% at 2 A g^{-1} (Fig. 8e). As shown in Fig. 8f, Wang *et al.*[87] used a mild KHCO$_3$ as the activating agent to generate nanopores within carbon nanoflakes (PCNFs) and investigated the effect of KHCO$_3$ on the activation process by adding the amount of activating reagent. It can be seen the nanoflakes with some folded morphology were interconnected with each other to form
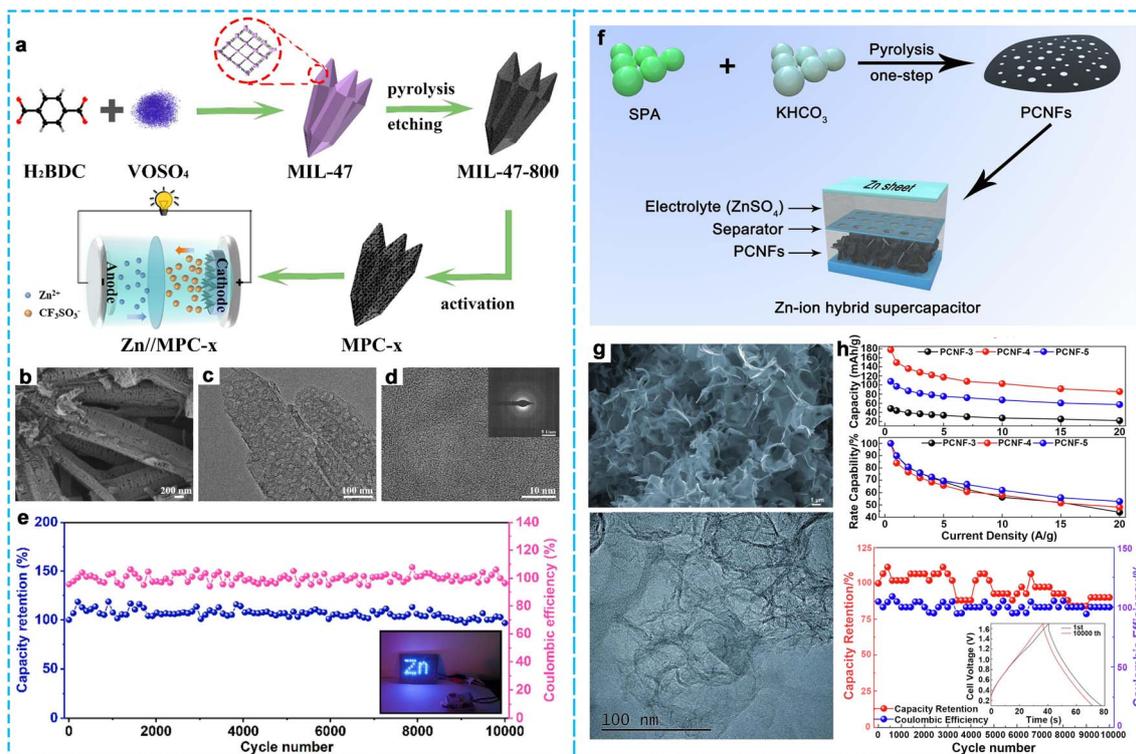
9408 | *J. Mater. Chem. A*, 2024, **12**, 9400–9420

This journal is © The Royal Society of Chemistry 2024

Fig. 8 (a) Schematic illustration of the preparation process of MPC, (b) SEM and (c and d) TEM images of MPC-2, and (e) cycling stability at 10 A g^{-1}.[85] Copyright 2022, Elsevier. (f) Schematic illustration of the synthetic process of PCNFs, (g) SEM and TEM images of PCNFs, and (h) electrical performance of PCNF cathode materials.[87] Copyright 2020, Elsevier.

a network structure (Fig. 8g). As demonstrated in Fig. 8h, the optimized PCNF-based ZHC device delivered a high specific capacitance (177.7 mA h g^{-1} at 0.5 A g^{-1}), excellent rate performance (85.5 mA h g^{-1} at 20 A g^{-1}), and outstanding cycling stability of 10 000 cycles (90% capacity retention at 10 A g^{-1}). More importantly, the ZHC exhibited a high energy density of 142.2 W h kg^{-1} at 400.3 W kg^{-1} and retained 68.4 W h kg^{-1} even at the maximum power density of 15 390 W kg^{-1}. The activation method is easy to operate, which is suitable for preparing hierarchically porous carbon materials with high SSA and pore volume, thus obtaining a high performance in Zn ion energy storage devices.

Considering environmental factors, biomass-derived porous carbon has attracted increasing attention due to its low cost and facile preparation.[88] For instance, bagasse and coconut shells can be mixed to prepare carbon materials. Liang's group[89] synthesized hierarchical porous carbon (HPC) with a 3D interconnected structure through a hydrothermal-assisted molecular-scale mixing strategy (Fig. 9a). The HPC showed a higher SSA, a large pore volume, and better electric conductivity than that of porous carbon derived from cellulose-rich bagasse (PC-B) and lignin-rich coconut shell (PC-CS). Consequently, the HPC cathode exhibited higher specific capacities than PC-CS and PC-B cathodes at different current densities. The HPC-based ZHC exhibited an ultrahigh capacity of 305 mA h g^{-1}, high energy density of 118.0 W h kg^{-1}, and excellent cycling stability for up to 20 000 cycles with over 94.9%

capacity retention at 2 A g^{-1}, which was superior to the commercial microporous carbon (YP-50)-based ZHCs. Zhang et al.[48] fabricated porous carbon derived from pencil shavings (PSC-Ax, where x corresponds to the temperature) by KOH-assisted activation at the required temperature (Fig. 9b). PSC-A600 materials can provide a large SSA (948 m^2 g^{-1}) and numerous active sites for the adsorption of ions by temperature optimization. As a result, the assembled Zn//PSC-A600 in 1 M Zn(CF$_3$SO$_3$)$_2$ electrolyte exhibited a specific capacitance of 413.3 F g^{-1} at a mass loading of 2.0 mg cm^{-2} and a high areal capacity of ~4.5 F cm^{-2} even at an ultrahigh loading of 24 mg cm^{-2}. Meanwhile, it also achieved a high energy density of 147.0 W h kg^{-1} at 136.1 W kg^{-1}, maximum power density of 15.7 kW kg^{-1} at 65.4 W h kg^{-1}, and superb durability over 10 000 cycles with 92.2% initial capacity retention at a high current density of 10 A g^{-1}. Notably, the ex situ experiments and theoretical calculations (Fig. 9c) were performed to investigate the energy storage process in Zn(CF$_3$SO$_3$)$_2$-based electrolyte, which was the typical adsorption/desorption of electrolyte ions and the reversible precipitation/dissolution of 2[Zn(CF$_3$SO$_3$)$_2$Zn(OH)$_2$]·3H$_2$O cluster, respectively. More importantly, when applying the PSC-A600 cathode in quasi-solid-state ZHCs with a unique anti-freezing hydrogel electrolyte (Fig. 9d), the flexible device could well perform at various bending states and maintain about 63.9% of its initial capacitance (20 °C) and ~100% coulombic efficiency after 80 cycles even at the relatively low temperature of −15 °C. As can be seen from the above-mentioned results,

This journal is © The Royal Society of Chemistry 2024

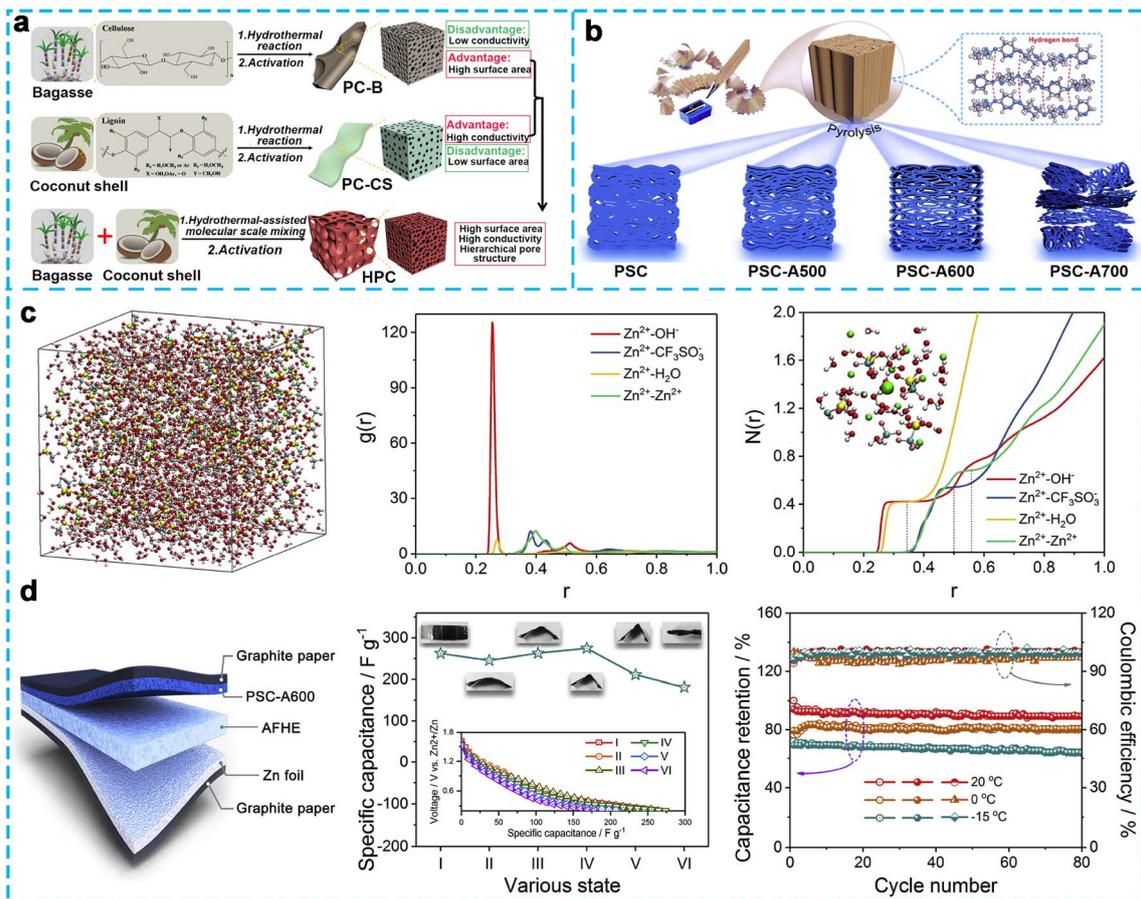J. Mater. Chem. A, 2024, 12, 9400–9420 | 9409

Fig. 9 (a) Schematic of the PC-B, PC-CS, and HPC synthetic processes.[89] Copyright 2019, Elsevier. (b) Schematic preparation of PSC and PSC-Ax, (c) theoretical calculations on the specific composition of byproduct generated in $Zn(CF_3SO_3)_2$-based electrolyte, and (d) electrochemical performance of the as-assembled quasi-solid-state Zn//PSC-A600.[48] Copyright 2020, Elsevier.

biomass-derived porous carbon should receive increasing attention because it is not only environmentally friendly but also has a high surface area and porosity, which facilitates ion transport to realize ZHCs with excellent electrochemical performances.

Designing oxygen-rich porous carbon is another effective strategy to realize satisfactory electrochemical performance. For example, Yin *et al.*[90] prepared oxygen-rich porous carbon (PC) by directing the pyrolysis of pyromellitic acid tetra-potassium salt with acid etching (Fig. 10a–d). PC800 possessed a large SSA of 1094.7 m^2 g^{-1}, pore volume of 1.11 cm^3 g^{-1}, and high oxygen content of 6.7 at% (Fig. 10e and f). In 3 M $Zn(ClO_4)_2$ aqueous electrolyte, the assembled ZHC with PC cathode and Zn anode showed a high capacitance of 340.7 F g^{-1} in a wide voltage window of 0–1.9 V (Fig. 10g), high energy density of 104.8 W h kg^{-1} at 58 W kg^{-1}, large power density of 48.8 kW kg^{-1} at 40.4 W h kg^{-1}, and excellent cycling stability over 30 000 cycles with a high capacity retention of 99.2%. This excellent performance was attributed to the highly reversible hydrogen and oxygen redox reactions on the porous carbon besides the typical EDLC (Fig. 10h–j). It is known that oxygen functional groups can offer additional pseudocapacitance to enhance the overall performance of ZHCs. Based on this, Wang *et al.*[91]

investigated the synergistic mechanism between the material structure and oxygen functional groups during the charge/discharge process. The oxygen-functionalized hierarchical porous carbon (HPC) materials were constructed *via* the pyrolysis of potassium citrate followed by acid etching. Benefiting from its high SSA (1259.7 m^2 g^{-1}), suitable micro-/mesopores structure, and high oxygen content (5.86%), the ZHCs based on HPC cathode exhibited a high capacity of 169.4 mA h g^{-1}, maximum energy density of 125.1 W h kg^{-1} at 0.1 A g^{-1} and ultrahigh power density of 16.1 kW kg^{-1} at 20 A g^{-1}. Especially, an ultralong cycle lifespan of up to 60 000 cycles at a high current density of 10 A g^{-1} with a high capacity retention of 93.1% could be obtained. The authors demonstrated that the oxygen functional groups (hydroxyl and carboxyl groups) can undergo reversible Faraday reactions with zinc ions to form C–O–Zn and C–OO–Zn by using *ex situ* measurements, which could effectively boost the performance of ZHCs during charge/discharge processes. Alternatively, the by-products of $Zn(CF_3-SO_3)_2$ $[Zn(OH)_2]_3 \cdot xH_2O$ caused capacity fading during cycling due to the effect of ion adsorption/desorption on the HPC cathode. Furthermore, the corresponding quasi-solid ZHC (Zn//gelatin/$Zn(CF_3SO_3)_2$//HPC) device also showed a satisfactory rate performance and cycling stability. Meanwhile, He *et al.*[92]

9410 | *J. Mater. Chem. A*, 2024, **12**, 9400–9420

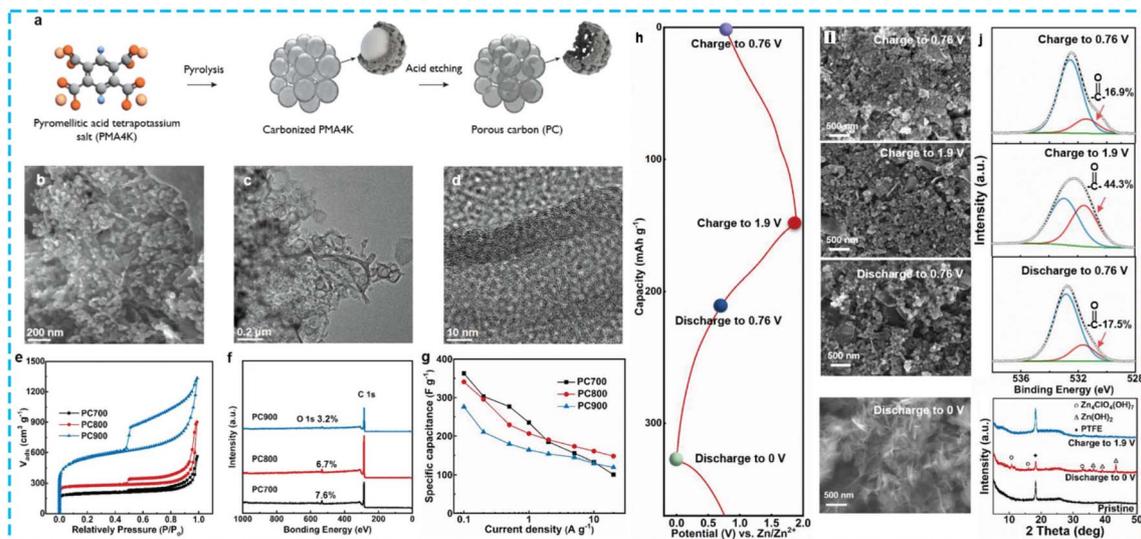This journal is © The Royal Society of Chemistry 2024

Fig. 10 (a) Schematic of the synthetic process of PC, (b) SEM and (c and d) TEM images of PC800, (e) N_2 adsorption–desorption isotherms, (f) XPS survey spectra, and (g) rate capability of PC cathodes. (h–j) Study of charge storage mechanism of PC800 cathode.[90] Copyright 2020, Wiley-VCH.

employed electrospinning and acid-assisted oxidation technology to synthesize an oxygen-enriched super hydrophilic, flexible porous carbon fiber (OPCNF-20) with super-hydrophilic character. As expected, the OPCNF-20 cathode-based ZHCs displayed a high energy density of 97.74 W h kg^{-1}, power density of 9.92 kW kg^{-1}, and ultralong-term cycling stability (retention rate of 81% after 50 000 cycles at 5 A g^{-1}).

Porous carbon materials were introduced based on specific aspects including their morphologies, SSA, porous structures, synthesis approaches, and electrochemical performances. Importantly, oxygen-rich porous carbon can significantly improve the performance of ZHCs by coupling EDLC and the reversible redox reaction of oxygen functional groups. Meanwhile, facile and green preparation processes are encouraged to be deeply studied to meet the requirements of high efficiency and environmental friendliness. Table 1 presents a summary of the electrochemical performances of porous carbon and AC cathode materials used in ZHCs, guiding the selection of suitable carbon cathode materials.

3.4 Heteroatom-doped carbon

Heteroatom-doped carbon materials have been widely applied in many fields, such as batteries, SCs, and the oxygen reduction reaction.[93] Recently, heteroatom-doped carbon materials have attracted increasing attention due to the fact that heteroatoms can introduce more active sites, enhance the electronic mobility, improve the wettability, and adjust the electrical and chemical properties of the carbon surface, showing great potential in enhancing the performance of ZHCs.[94] Therefore, we summarize the synthesis strategies, doping content, and electrochemical properties of heteroatom-doped carbon cathodes, including single-doped (N, S, P, B, etc.), dual-heteroatom-doped-and triple-heteroatom-doped carbon materials. Besides, we analyze the relationship between heteroatom-doped and

electrochemical performance and their working principles. However, O atoms can inevitably be observed in most materials because of the experimental conditions and other unavoidable external factors.[93] Herein, we define carbon materials with a high oxygen content as single-doped or multiple-doped carbons, as described in the literature.

Single-doped carbon materials, especially nitrogen (N) doped materials are commonly studied because they are next to the carbon atom in the periodic table and are relatively easy to bond with carbon chemically.[95–97] Lu et al.[97] designed N-doped hierarchically porous carbon (HNPC) using zeolite NaY as the template and furfuryl alcohol as the carbon source and subsequent thermal treatment to introduce N dopants and hierarchical pores (Fig. 11a). The SSA of HNPC was up to 2762.7 m^2 g^{-1} and the N content was 2.21%, thus increasing the surface wettability (the contact angle decreased from 140° to 76°), the conductivity and active sites, which could produce pseudocapacitance (Fig. 11b). Importantly, not only a series of ex situ measurements applied to study the relevant working principle but also DFT calculations were performed to investigate the effect of N atoms on the adsorption/desorption process of Zn ions at the HNPC/electrolyte interface. The results showed that the overall capacitance of Zn//HNPC was conjointly contributed by the typical EDLC and the additional pseudocapacitance via the chemical adsorption of Zn ions (C–OH + Zn^{2+} + e$^-$ ↔ C··· O···Zn + H$^+$). At the same time, N dopants could effectively lower the energy barrier of chemical interaction between C–O and Zn^{2+}, thus effectively boosting the chemical adsorption of Zn ions on the electrode surface (Fig. 11c). Consequently, the ZHCs based on the HNPC cathode in 1 M ZnSO$_4$ electrolyte exhibited an exceptionally high energy density of 107.3 W h kg^{-1} at 4.2 A g^{-1}, superb power density of 24.9 kW kg^{-1}, and ultralong-term lifespan over 20 000 cycles with high retention of 99.7% at a high current density of 16.7 A g^{-1}, which is superior to state-

This journal is © The Royal Society of Chemistry 2024

J. Mater. Chem. A, 2024, 12, 9400–9420 | 9411

Table 1 The electrochemical performances of the reported porous carbon and activated carbon-based cathodes in ZHCs

Materials	SSA $(m^2\ g^{-1})$	Electrolyte	Capacity	Energy density/W h kg^{-1}	Power density/kW kg^{-1}	Cycling stability	Ref.
AC	3384	1 M $Zn(CF_3SO_3)_2$	170 F g^{-1}/0.1 A g^{-1}	61.6	1.725	91%/20 000 cycles (2 A g^{-1})	23
AC	1990	2 M $ZnSO_4$	132 mA h g^{-1}/0.1 A g^{-1}	140.8	2.85	72%/20 000 cycles (4 A g^{-1})	33
AC	1923	2 M $ZnSO_4$	121 mA h g^{-1}/0.1 A g^{-1}	84	14.9	91%/10 000 cycles (1 A g^{-1})	46
HPAC	3525	3 M $Zn(CF_3SO_3)_2$	231 mA h g^{-1}/0.5 A g^{-1}	—	11.4	~70%/18 000 cycles (10 A g^{-1})	57
MSAC	2527	2 M $ZnSO_4$	176 mA h g^{-1}/0.5 A g^{-1}	188	10.666	78%/40 000 cycles (10 A g^{-1})	58
ACC	2619	2 M $ZnSO_4$	318 F g^{-1}/0.1 A g^{-1}	94	7	98.2%/10 000 cycles (5 A g^{-1})	64
CSAC	1260	3 M $Zn(ClO_4)_2$	423.5 F g^{-1}/0.1 A g^{-1}	190.3	24.5	—	65
ACC	745	1 M $ZnSO_4$/1 M Na_2SO_4	153 mA h g^{-1}/1 mA cm^{-2}	100	1.692	Stable cycling up to 20 000 cycles	120
AC	1386	2 M $ZnSO_4$	—	82.9	10	98.8%/5000 cycles (1 A g^{-1})	121
AC	—	2 M $ZnSO_4$	—	70.4	7.6	~100%/5000 cycles (2 A g^{-1})	122
PSC-A600	948	1 M $Zn(CF_3SO_3)_2$	413.3 F g^{-1}/0.2 A g^{-1}	147.0	15.7	92.2%/10 000 cycles (10 A g^{-1})	48
HCSs	819.5	1 M $ZnSO_4$	86.8 mA h g^{-1}/0.5 A g^{-1}	59.7	~9	98%/15 000 cycles (1 A g^{-1})	80
MCHS	1275	2 M $ZnSO_4$	174.7 mA h g^{-1}/0.1 A g^{-1}	129.3	13.7	96%/10 000 cycles (1 A g^{-1})	82
MPC-2	2125	3 M $Zn(CF_3SO_3)_2$	289.2 F g^{-1}/0.2 A g^{-1}	130.1	7.8	96.7%/10 000 cycles (10 A g^{-1})	85
PCNFs	1770	1 M $ZnSO_4$	177.7 mA h g^{-1}/0.5 A g^{-1}	142.4	15.39	90%/10 000 cycles (10 A g^{-1})	87
3D HPC	3401	2 M $ZnSO_4$/1 M Na_2SO_4	305 mA h g^{-1}/0.1 A g^{-1}	118.0	3.2	94.9%/20 000 cycles (2 A g^{-1})	89
PC800	1094.7	3 M $Zn(ClO_4)_2$	179.8 mA h g^{-1}/0.1 A g^{-1}	104.8	48.8	99.2%/30 000 cycles (20 A g^{-1})	90
HPC-600	1259.7	1 M $Zn(CF_3SO_3)_2$	169.4 mA h g^{-1}/0.1 A g^{-1}	125.1	16.1	93.1%/60 000 cycles (10 A g^{-1})	91
OPCNF-20	532.5	1 M $ZnSO_4$	136.4 mA h g^{-1}/0.1 A g^{-1}	97.74	9.92	81%/50 000 cycles (5 A g^{-1})	92

of-the-art ZHCs. Particularly, the quasi-solid-state Zn//HNPC in poly(vinyl alcohol) gel electrolyte still exhibited a sufficient capacity of 148.2 mA h g^{-1}, high energy density of 91.8 W h kg^{-1} and a remarkable power density of 27.6 kW kg^{-1}. This is an important study illustrating the energy storage mechanism of heteroatom doping to enhance the electrochemical
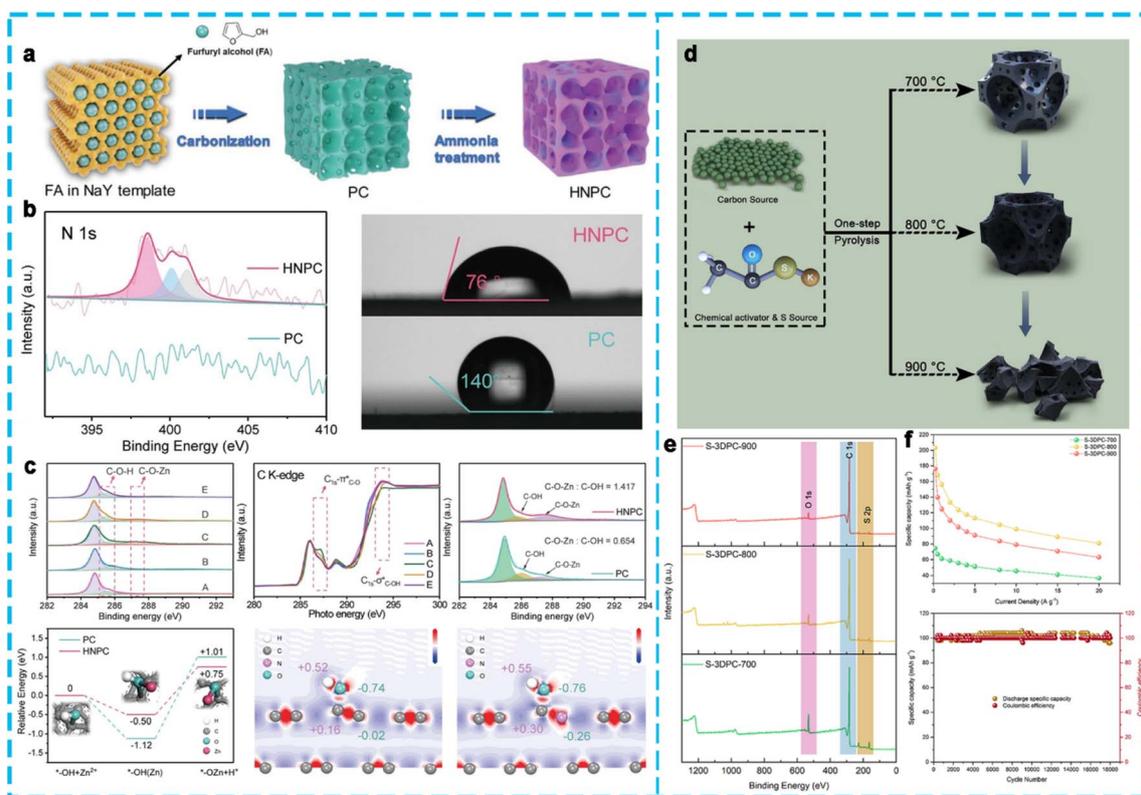

Fig. 11 (a) Schematic illustration of the synthetic procedure of HNPC, (b) high-resolution N 1s spectra, and contact angles of HNPC, respectively. (c) Study of the working principle of HNPC cathode.[97] Copyright 2019, Wiley-VCH. (d) Schematic illustration of the synthesis route of S-3DPCs, (e) XPS survey spectra of S-3DPCs obtained at different calcination temperatures, and (f) corresponding electrochemical performance.[100] Copyright 2021, Wiley-VCH.

9412 | *J. Mater. Chem. A*, 2024, **12**, 9400–9420

This journal is © The Royal Society of Chemistry 2024

performance of ZHCs. Subsequently, Liu et al.[98] prepared nitrogen-doped hierarchical porous carbon (N-HPC) via one-step method. Benefitting from the existence of micro–meso-pores and nitrogen doping, the ZHCs using N-HPC as the cathode manifested a high capacity of 136.8 mA h g^{-1} at 0.1 A g^{-1} (corresponding to an energy density of 191 W h kg^{-1} at 58.5 W kg^{-1}), large power density of 3633.4 W kg^{-1} and cycling stability of 5000 cycles with 90.9% capacity retention. Similar, diblock copolymer micelle-derived nitrogen-doped hierarchi-cally porous carbon spheres (N-HPCSs) with a N content of 4.32 at% were fabricated for ZHCs,[99] which delivered a high specific capacity (180.4 mA h g^{-1} at 0.5 A g^{-1}), excellent rate perfor-mance (58.3 mA h g^{-1} even at an extremely high current density of 100 A g^{-1}), high energy/power densities (144.3 W h kg^{-1}/79.9 kW kg^{-1}), and outstanding electrochemical durability with an exciting capacity retention of 98.2% after 50 000 cycles at 5 A g^{-1}, showing promising potential for practical applications. In addition, the highly reversible formation/dissolution processes of $Zn_4SO_4(OH)_6 \cdot 5H_2O$ indicated that the electro-chemical active sites on the N-HPCS surface were well retained according to the ex situ XRD tests. Another unique sulfur (S) doping has emerged and arousing interest in the research of ZHCs. Wang et al.[100] developed a versatile synthetic route for producing S-doped 3D porous carbon (S-3DPC-800) by employ-ing sustainable pine needles as the carbon source and potas-sium thioacetate as the activation agent without any additives (Fig. 11d). The prepared S-3DPC-800 showed a unique 3D architecture with a large specific surface area (2336.9 m^2 g^{-1}), abundant ions, accessible micropores/mesopores, and a certain amount of sulfur (1.71 at%, Fig. 11e). As a result, the ZHC device with S-3DPC-800 cathode in 2 M $ZnSO_4$ solution delivered a high specific capacity (203.3 mA h g^{-1} at 0.2 A g^{-1}), superior rate performance (81.0 mA h g^{-1} at 20 A g^{-1}), and outstanding cycling stability with 96.8% capacity retention after 18 000 cycles at 10 A g^{-1} (Fig. 11f). Moreover, it displayed a maximum energy density of up to 162.6 W h kg^{-1} (99.0 W h L^{-1}) at a power density of 160 W kg^{-1} (97.4 W L^{-1}). It can be seen that heteroatom-doped carbon materials exhibit excellent capacitive behavior in ZHC devices.

Compared with single-heteroatom doping, dual- and triple-heteroatom doping can significantly change the electronic structure of carbon via their synergistic coupling effects. Zhao et al.[47] fabricated N, O co-doped hierarchical porous carbon (HPC), integrated with flexible carbon cloth (CC) through a drop-coating and carbonization approach as the cathode material for ZHSs. Benefiting from the high SSA (197.45 m^2 g^{-1}), suitable pore size distribution, interconnected conductive network, and N/O dual-doped (N: 6.52 at%, O: 3.76%), the HPC/CC-based ZHS delivered a high specific capacity of 138.5 mA h g^{-1} at 0.5 A g^{-1} and superb rate performance of 75 mA h g^{-1} even at a high current density of 20 A g^{-1}. There-fore, this device achieved an energy density of 110 W h kg^{-1} at 499 W kg^{-1}, maximum power density of 20 kW kg^{-1}, and excellent cycling stability without decay after 10 000 cycles at 5 A g^{-1}. More importantly, they first proposed the dual cation (H$^+$ and Zn^{2+}) chemical absorption process for extra energy storage capacity and verified it by ex situ experiments (C···O +

Zn^{2+}/H$^+$ + e$^-$ ↔ C···O···Zn/C···O···H and N···O + Zn^{2+}/H$^+$ + e$^-$ ↔ N···O···Zn/C···O···H). Also, they explained the precipitation/dissolution process of zinc hydroxide sulfate hydrate, which was deemed a partial source of energy storage capacity. The O dopants can be used as the active sites for pseudocapacitance, while N atoms can facilitate the physical/chemical adsorption and desorption processes. Similarly, Lu et al.[101] proposed the preparation of N/S co-doped carbon materials (NPC) derived from pitch, in which the N dopants could participate in the surface redox reaction to provide extra Zn ion storage ability and improve the electrochemical kinetics. Consequently, the NPC//Zn ZHCs delivered a high capacity of 136.2 mA h g^{-1}, satisfac-tory rate performance (50.8% capacity retention from 0.3 A g^{-1} to 15 A g^{-1}), and excellent anti-self-discharge ability (95.6% capacity retention after 24 h of rest). For the anti-self-discharge, Dong group[102] also realized high-energy and anti-self-discharge ZHSs based on fibrous carbon cathodes with a hierarchically porous surface and O/N heteroatom functional groups.

Compared to carbon, phosphorus (P) possesses a low elec-tronegativity and high electron-donating ability, while boron (B) has higher electronic conductivity due to the shift in its Fermi level to the conducting band.[103] Thus, Xu group[104] reported a green gas-steamed MOF approach to preparing open-wall carbon cages, while simultaneously offering N, P dopants functionalized in the carbon matrix (OCCs) in a one-step process, while the content of doped N, P in OCCs was as high as 2.53 and 2.96 at%, respectively. The OCCs with unique open-wall structure and hierarchical micro/meso/macropore struc-ture could provide more channels for high-speed mass trans-port of reactants to the accessible active sites, while the N/P dual-doping could effectively lower the energy barrier of the chemical interaction between the carbon surface and Zn^{2+}, further boosting the chemical adsorption of Zn ions on the carbon surface. Also, according to their report, the electrons of the adjacent C atoms tend to flow toward the N/P atoms with higher electronegativity. The C atoms function more like elec-tron acceptors with respect to the nearby O atoms, and thus the resultant electron-withdrawing inductive effect promotes the formation of C–O–Zn bonds. Another possible pathway is that the sulfur functional groups (such as –PO$_3^-$) can directly facil-itate the chemical adsorption of Zn ions. As a result, the OCC-based ZHC coin-type cells displayed a wide operating voltage of 2.0 V, high specific capacity of 225 mA h g^{-1} at 0.1 A g^{-1}, and ultralong cycling life of up to 300 000 cycles with a superb capacity retention of 96.5% even at a high current density of 50 A g^{-1}. Based on the superior performance of the OCC cathode, a soft-pack ZHSC device was fabricated, which showed a high energy density of 97 W h kg^{-1} and superb power density of 6.5 kW kg^{-1}. More importantly, the soft-pack device could operate in a wide temperature range of −25 to +40 °C, holding tremendous possibilities for practical applications in everyday life. Also, heteroatom doping can efficiently improve the pseu-docapacitance of carbon cathodes. Zhang and co-workers[105] designed carbon clusters assembled with P/N dual-doped hollow nanospheres (PN-CHoNS) via a dual-functional manga-nese oxide nanoflower template-induced strategy and subse-quent carbonization treatment (Fig. 12a). The ZHCs using the

This journal is © The Royal Society of Chemistry 2024

J. Mater. Chem. A, 2024, 12, 9400–9420 | 9413

PN-CHoNS cathode delivered a high specific capacity of 164.4 mA h g^{-1} at 0.2 A g^{-1}, superior rate performance with a retained capacity of 66.7 mA h g^{-1} at 40 A g^{-1}, exceptional energy density of 116.0 W h kg^{-1} at 141 W kg^{-1} and maximum power density of 21 660 W kg^{-1} with a decent energy density of 36.1 W h kg^{-1}, as well as ultra-long cycling stability of 12 000 cycles with a capacity retention of 80.6%, which was superior to the control sample (Fig. 12b). The excellent electrochemical performance was attributed to the unique features of the 3D nanosphere with a porous structure for ion/electron transfer, hollow interior for good electrolyte/electrode contact, and shortened ion transfer path, as well as the dual-doping engineering electronic structure. Especially, the DFT calculation results (Fig. 12c) revealed that P/N dual-doping could effectively boost the chemical absorption/desorption kinetics of Zn ions, which is favorable for the high electrochemical property of ZHCs. Sun et al.[107] proposed that N and P dopants are energetically favorable for promoting the chemical adsorption process of Zn^{2+} on the cathode interface according to theoretical simulations. Alternatively, N and B dual-doping has also been regarded as an effective strategy to enhance the energy storage performance of carbon cathodes. For instance, Lu et al.[108] designed layered B/N co-doped porous carbon (LDC) guided by facile retention after 6500 cycles at 5 A g^{-1}. Soon afterward, Pan et al.[109] designed a hierarchically porous B, N dual-doped carbon by thermally annealing metal–organic frameworks and boric

acid. The obtained B, N dual-doped carbon showed high heteroatom contents (3.82 at% B and 6.4 at% N), high SSA of 926.67 m^2 g^{-1}, and abundant hierarchical pore structure (micropore, mesopore, and macropore), which benefitted the electrochemical performance. Alternatively, B, N dual doping could significantly influence the electronic structure and density state of the carbon surface, thus enhancing the pseudocapacitance contribution. As a result, the B, N dual-doped carbon cathode exhibited a high energy density of 115.7 W h kg^{-1} at 711.6 W kg^{-1} in the voltage range of 0.2–1.8 V and a superior cycling stability with 99.2% capacity retention after 10 000 cycles.

Triple-heteroatom doping has been researched due to the success of dual-doped carbon cathode materials. For example, Fan et al.[106] synthesized a B, N, and O co-doped flower-like carbon (BCF) via the spheroidizing growth of hydrothermal carbon as an assembly drive and in situ-formed melamine cyanurate nanosheets as structure-directing agent (Fig. 12d–f). The contents of N, O, and B on the surface of BCF were 7.43%, 6.59%, and 0.79%, respectively. As presented in Fig. 12g, N-doping could enhance the electronic conductivity and was prone to providing pseudo-capacitance as an electron donor, B-doping with electron deficiency was favorable to improve the chemical adsorption of SO$_4$$^{2-}$ on the carbon cathode surface (B + SO$_4$$^{2-}$ ↔ B^{2+}//(SO$_4$)$^{2-}$), while O-doping can react with Zn ions to provide additional
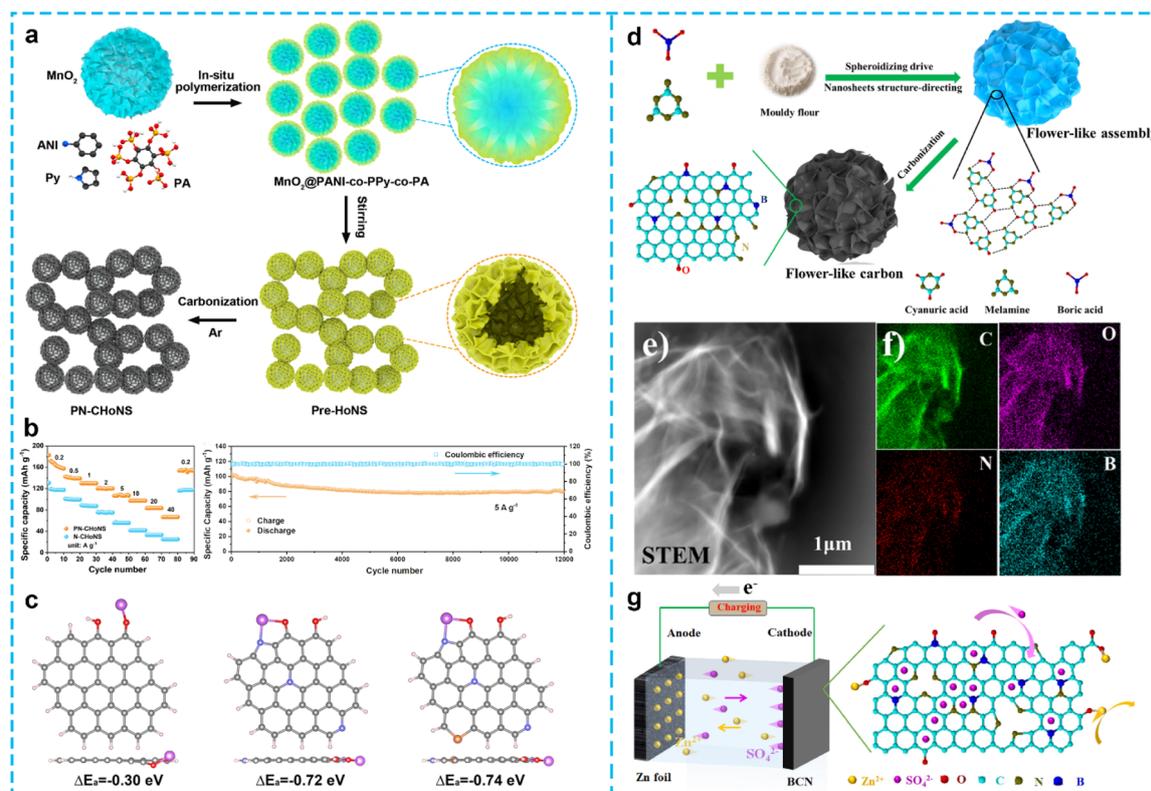

Fig. 12 (a) Schematic illustration of the formation process of PN-CHoNS, (b) electrochemical performance of PN-CHoNS cathode–based ZHCs, and (c) DFT calculation.[105] Copyright 2021, Elsevier. (d) Preparation process of BCF, (e–f) elemental mapping images of BCF, and (g) schematic working mechanism of the aqueous BCF-based ZHC device during the charging process.[106] Copyright 2021, Elsevier.

9414 | J. Mater. Chem. A, 2024, 12, 9400–9420

This journal is © The Royal Society of Chemistry 2024

Table 2 Performance comparison of the reported ZHCs with heteroatom-doped carbon cathodes

Materials	SSA ($m^2\,g^{-1}$)	Electrolyte	Capacity	Energy density/W h kg^{-1}	Power density/kW kg^{-1}	Cycling stability	Ref.
HNPC	2762.7	1 M ZnSO4	177.8 mA h g^{-1}/ 4.2 A g^{-1}	107.3	24.9	99.7%/20 000 cycles (16.7 A g^{-1})	97
		PVA gel	148.2 mA h g^{-1}/ 4.2 A g^{-1}	91.8	27.6	88.3%/10 000 cycles	
N-HPC	879	2 M $ZnSO_4$	136.8 mA h g^{-1}/ 0.1 A g^{-1}	191	3.633	90.9%/5000 cycles (1 A g^{-1})	98
N-HPCS	789.2	2 M $ZnSO_4$	180.4 mA h g^{-1}/ 0.5 A g^{-1}	144.3	79.9	98.2%/50 000 cycles (5 A g^{-1})	99
S-3DPC-800	2336.9	2 M $ZnSO_4$	203.3 mA h g^{-1}/ 0.2 A g^{-1}	162.6	16	96.8%/18 000 cycles (10 A g^{-1})	100
NPC	1707	1 M $ZnSO_4$	136.2 mA h g^{-1}/ 0.2 A g^{-1}	81.1	12.8	98.9%/60 000 cycles (10 A g^{-1})	101
N/O co-doped HPC/CC	197.45	2 M $ZnSO_4$	138.5 mA h g^{-1}/ 0.5 A g^{-1}	110	20	104.3%/10 000 cycles (5 A g^{-1})	47
BGC-750	3657.5	3 M $Zn(CF_3SO_3)_2$	257 mA h g^{-1}/ 0.5 A g^{-1}	168	61.7	—	123
HPCF (O/N heteroatom)	2000	2 M $ZnSO_4$	141 mA h g^{-1}/ 0.1 A g^{-1}	112	14.5	93%/6000 cycles (20 A g^{-1})	102
N, P-doped OCC-900	1733	Saturated $Zn(CF_3SO_3)_2$	225 mA h g^{-1}/ 0.1 A g^{-1}	—	—	96.5%/300 000 cycles (50 A g^{-1})	104
			167 mA h g^{-1}/ 0.1 A g^{-1}	97	6.5	—	
PN-CHoNS	29.7	2 M $ZnSO_4$	164.4 mA h g^{-1}/ 0.2 A g^{-1}	116.0	21.66	80.6%/12 000 cycles (5 A g^{-1})	105
CNPK	2038	1 M $ZnSO_4$	103.2 mA h g^{-1}/ 0.1 A g^{-1}	81.1	13.366	100%/10 000 cycles (5 A g^{-1})	107
B/N co-doped LDC	597	1 M $ZnSO_4$	127.7 mA h g^{-1}/ 0.5 A g^{-1}	97.6	12.1	—	108
		Gelatin/$ZnSO_4$ (gel)	116.8 mA h g^{-1}/ 0.5 A g^{-1}	86.6	12.2	81.3%/6500 cycles (5 A g^{-1})	
BN-ZIC-3	926.67	2 M KOH and 2 M $ZnSO_4$	162.6 mA h g^{-1}/ 1 A g^{-1}	115.7	—	99.2%/10 000 cycles (10 A g^{-1})	109
B, N and O co-doped flower-like carbon	282	2 M $ZnSO_4$	133.5 mA h g^{-1}/ 1 A g^{-1}	119.7	16.5	92%/20 000 cycles (10 A g^{-1})	106
N, F, O-doped carbon (R6)	3354.9	2 M $Zn(CF_3SO_3)_2$	168.4 mA h g^{-1}/ 0.5 A g^{-1}	131.9	30.8	~100%/12 000 cycles (10 A g^{-1})	110

pseudocapacitance ($C-O-Zn \leftrightarrow C-O-Zn^{2+} + 2e^-$). Consequently, the BCF-based ZHC delivered a specific capacity of 133.5 mA h g^{-1} at 1 A g^{-1} and a high preservation of 70 mA h g^{-1} at 20 A g^{-1}. Especially, the device achieved a superior energy density of 119.7 W h kg^{-1} at 890 W kg^{-1}, large power density of 16.5 kW kg^{-1} even at 63.5 W h kg^{-1}, and outstanding cycle life of 20 000 cycles with 92% retention at 10 A g^{-1}. However, the preparation of carbon precursors usually requires tedious steps, and thus Zhu and co-workers synthesized N, F, and O-doped carbon materials *via* a straightforward and scalable one-step method.[110] The obtained N, F, and O-doped carbons possessed a high SSA (~1700 $m^2\,g^{-1}$ to ~3300 $m^2\,g^{-1}$) and regulated pore distribution (0.87 $cm^{-3}\,g^{-1}$ to 2.26 $cm^{-3}\,g^{-1}$). Heteroatom doping can improve the electrolyte surface wettability and enhance the number of electrochemical pseudocapacitance active sites. Therefore, the ZHCs using N, F, O-doped carbon as the cathode and zinc foil as the anode in 2 M $Zn(CF_3SO_3)_2$ electrolyte exhibited a high energy density of 131.9 W h kg^{-1} at 0.5 A g^{-1} and highest power density of 30.8 kW kg^{-1} at

40 A g^{-1}. Besides, an excellent cycling performance at 10 A g^{-1} over 12 000 cycles with almost no capacity fading was achieved. To better compare the effects of heteroatom doping on carbon cathode materials for ZHCs, we summarize the performances of heteroatom-doped carbon materials in Table 2.

4. Research progress of electrolytes

The electrolyte also plays an important role in ZHCs, which can greatly affect their energy density, cyclic stability, and rate performance, thus receiving considerable attention in recent years. In the process of continuous research and development, various electrolytes for ZHCs have been designed and prepared, including aqueous electrolytes, organic electrolytes and some other electrolytes, exhibiting a superior Zn ion storage performance. In this section, the recent advances in aqueous electrolytes, organic electrolytes and some other electrolytes in ZHCs will be introduced.

This journal is © The Royal Society of Chemistry 2024

J. Mater. Chem. A, 2024, **12**, 9400–9420 | **9415**

4.1 Aqueous electrolytes

In recent years, aqueous electrolytes have been extensively explored and used in ZHCs by virtue of their low cost, high safety and environmentally friendly nature, which generally include $ZnSO_4$, $Zn(CF_3SO_3)_2$, $ZnCl_2$, $Zn(CH_3COO)_2$ and $Zn(ClO_4)_2$.[111] Chen et al. systematically researched several standard Zn salt aqueous electrolytes ($ZnCl_2$, $ZnSO_4$, $Zn(CF_3SO_3)_2$, $Zn(Ac)_2$, and $Zn(NO_3)_2$) by comparing their physicochemical properties and electrochemical properties for ZHCs. Based on the Nyquist curves of ZIHCs, the Zn ion diffusion resistance followed the order of $ZnCl_2 < Zn(CF_3SO_3)_2 < ZnSO_4 < Zn(Ac)_2 < Zn(NO_3)_2$. As a result, benefitting from its fastest ion diffusion rate, the ZHCs using $ZnCl_2$ electrolyte displayed the best capacitance among all the prepared electrolytes, followed by $ZnSO_4$, $Zn(CF_3SO_3)_2$, $Zn(Ac)_2$, and $Zn(NO_3)_2$ electrolyte. The resulting ZIHCs by employing $ZnCl_2$ electrolyte could deliver a high energy density of up to 217 W h kg^{-1} at a power density of 450 W kg^{-1} and a long cycling life of over 100 000 cycles. Also, the device could manifest outstanding low-temperature adaptability and mechanical flexibility.[112] Furthermore, Zhang et al. designed a hybrid supercapacitor with different Zn-based aqueous electrolytes ($ZnCl_2$, $Zn(SO_4)_2$, $Zn(NO_3)_2$, $Zn(CH_3COO)_2$, and $Zn(CF_3SO_3)_2$). By comparing the morphology and phase evolution of the deposits during the Zn plating processes in these electrolytes, the employment of 3 M $Zn(CF_3SO_3)_2$ electrolyte could efficiently achieve a high Zn stripping/plating efficiency, resulting in an excellent electrochemical performance.[70] Besides, Qiu et al. prepared a low-concentration 3 M $Zn(ClO_4)_2$ aqueous electrolyte with a high ionic conductivity even at an ultralow temperature. The spectroscopic characterization and theoretical simulation disclosed that the solvation structure (Zn^{2+} ion in the electrolyte) could effectively destroy the hydrogen bond network between water molecules to offer an electrolyte with a lower freezing point. This zinc-ion hybrid capacitor with designed low-temperature electrolyte exhibited a high energy density of 40.91 W h kg^{-1} at -60 °C and a long-cycle life after 200 days at -30 °C, which provides more enlightenment to explore electrolytes for low-temperature electrochemical energy storage device.[113] Moreover, Zhang et al. assembled a Zn ion hybrid capacitor device with sulfur-doped carbon cathode, Zn foil anode and 2 M $ZnSO_4$ solution as the electrolyte, which displayed a high power density of 19 170 W kg^{-1} and long cycling performance over 25 000 cycles at 5.0 A g^{-1}.[114]

4.2 Organic electrolytes

Aqueous electrolytes have made considerable progress in recent years; however, their narrow voltage window and possible water decomposition during cycling are still unsatisfactory, which limits their long-term development. Recently, organic electrolytes have gradually attracted attention due to their high chemical stability, wide operating temperature range and good ionic conductivity, which can provide a wider operating voltage range and achieve a higher energy/power density.[115] For example, Wang et al. designed a Zn ion hybrid supercapacitor with a porous carbon cathode, Zn anode and organic N,N-dimethylformamide (DMF)-containing Zn trifluoromethanesulfonate (Zn-TFMS) electrolyte. The formation of a Zn^{2+}–DMF complex in the electrolyte could facilitate smooth deposition, avoid the issue of undesirable H_2 evolution and improve dendrite-free Zn plating/stripping. As a consequence, the device exhibited a high capacitance retention of 69% from 1 mg cm^{-2} to 40 mg cm^{-2} mass loading, a long life of 9000 cycles with a high mass loading of 10 mg cm^{-2} and an energy density of 25.9 W h kg^{-1} at 40 mg cm^{-2}, which is much better than that in previous reports. More importantly, this hybrid supercapacitor still presented electrochemical properties within a wide temperature range of -65 °C to 100 °C due to the high boiling point and low freezing point characteristic of DMF.[116] Besides that, Zhi et al. recently constructed a zinc ion hybrid capacitor device, where the organic electrolyte was prepared by adding 0.2 M $ZnCl_2$ to tetraethylammonium tetrafluoroborate in propylene carbonate (Et_4NBF_4/PC) solvent. Benefiting from the mutual effect of highly concentrated salt and Et_4NBF_4/PC, which can enhance the voltage window ceiling and cycling life, an excellent electrochemical performance was realized. Thus, the capacitors displayed a higher operating voltage of up to 2.5 V and a high capacity of 105.9 F g^{-1} even after 9500 cycles. Notably, the organic solvent could also be utilized as the electrolyte additive to achieve high-performance ZHCs. Shi et al. used anthraquinone compounds as electrolyte additives to enable the favorable solvation of Zn^{2+} and boost the pseudocapacitive behavior, and the assembled device displayed an enhanced capacity of 195.0 mA h g^{-1} and improved cycling stability.[117]

4.3 Other electrolytes

Besides the above-mentioned aqueous and organic electrolytes, some other electrolytes have also been developed and employed in ZHCs, including ionic liquid electrolytes, polymer electrolytes, and gel electrolytes, due to their different compositions and structural characteristics. For instance, Yan et al. designed a new Zn salt-based ionic liquid electrolyte composed of $Zn(BF_4)_2$ and [EMIM]BF_4 to assemble a Zn ion hybrid capacitor with three-dimensional activated carbon (3D-AC) as the cathode and Zn foil as the anode. The $Zn(BF_4)_2$//[EMIM]BF_4 electrolyte possessed high reductive/oxidative stability, which could reduce the irreversible formation of dendrites and side reactions during the cycling process to accelerate Zn plating/stripping. Finally, the designed device with $Zn(BF_4)_2$//[EMIM]BF_4 electrolyte showed a superior performance with a high average output voltage (1.9 V), high energy/power density (220 W h kg^{-1}/9.5 kW kg^{-1}), and long cycle life (95% capacity retention after 20 000 cycles). In the case of gel electrolytes, unlike the traditional liquid electrolytes, the electrolyte can be fixed in the electrode aperture to avoid the leakage and volatilization of liquid electrolytes. Besides, gel electrolytes possess high safety, high conductivity, high energy density and long cycling life, manifesting their huge development potential.[118] Cui et al. designed and prepared a polyanion-induced single zinc-ion gel polymer electrolyte (GPE) by utilizing 2-acrylamido-2-methylpropanesulfonic acid (AMPS) as the raw material, exhibiting good interfacial adhesion and mechanical

9416 | J. Mater. Chem. A, 2024, 12, 9400–9420

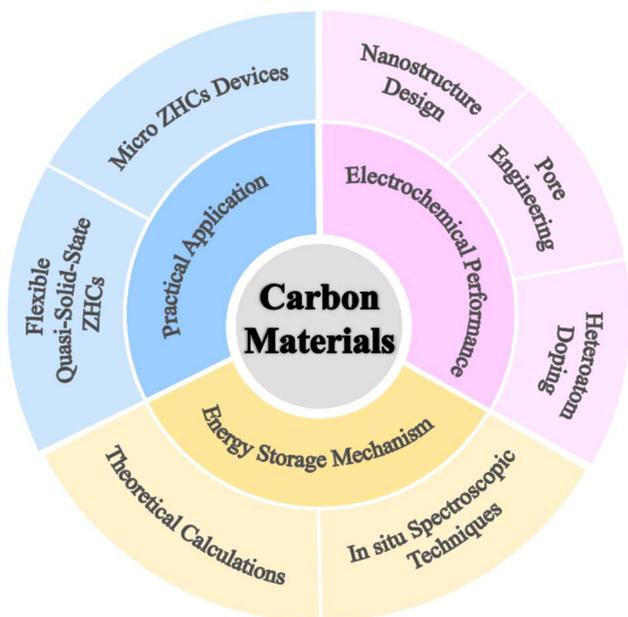This journal is © The Royal Society of Chemistry 2024

Fig. 13 Remaining challenges and prospects of carbon cathode materials for ZHCs.

strength to enhance the overall electrochemical performance. Finally, the assembled ZIHC showed a high energy density of 140 W h kg^{-1} and outstanding cycling life even at −20 °C and 60 °C (93.1% and 84.2% capacity retention), respectively. Furthermore, after undergoing a long lifespan over 5000 cycles, the electrodes still showed excellent compatibility and interface stability with the GPE.[119] It is believed that under continuous research development and innovation, gel electrolyte-based ZHCs will achieve a higher energy density, longer cycle life and better safety performance, creating a greater prospect for development.

5. Conclusions and prospects

In summary, ZHCs have attracted increasing attention due to their low cost, environmentally friendly nature, high energy/power density, and ultra-long cycle lifespan, making them highly promising for practical applications. Electrodes play an important role in the electrochemical performance of ZHCs, with carbon materials being a hot research topic due to their high-performance potential. This review summarized the recent progress in various carbon cathode materials, including AC, graphene, porous carbon, and heteroatom-doped carbon materials used in ZHCs. It covered their synthesis, morphology, electrochemical performance, and possible charge storage mechanism. Despite the considerable progress in advanced ZHCs, research on carbon cathodes is still in its infancy. The remaining challenges and prospects for ZHCs can be summarized as follows (Fig. 13).

(1) Improving the electrochemical performance of carbon cathode materials: the specific capacity of carbon cathode materials fails to match the high theoretical capacity of Zn electrodes, leading to the unsatisfactory performance of ZHCs. Therefore, effective modification strategies are urgently needed

to achieve high-performance devices. These include nanostructure design, pore engineering, and heteroatom doping.

(2) Exploring the detailed energy storage mechanism of carbon cathode-based ZHCs: the storage capacitance is mainly contributed by EDLC storage with ion adsorption/desorption at/near carbon surface and pseudocapacitance by reversible faradaic surface reactions. However, the electrochemical mechanism of carbon cathode-based ZHCs is not sufficiently understood, especially heteroatom-doped carbon. Alternatively, although theoretical calculations have been applied to understand the storage mechanisms based on the theoretical model of graphene, the model is not entirely consistent with the real-world situation. Therefore, efforts should be made to investigate the electrochemical behaviors of electrodes in ZHCs during energy storage using advanced *in situ* technologies combined with theoretical calculations based on more reasonable models.

(3) Considering the practical application of ZHCs: in addition to coin cells of ZHCs, multifunctional zinc ion energy storage devices (such as flexible quasi-solid-state ZHCs and micro devices) should be constructed to keep up with the demands of society. For example, flexible ZHCs play a critical role as a safe power source in realizing wearable electronic products. Soft/flexible electrodes must be developed to cater to various on-demand applications for flexible ZHCs or micro devices, achieving wide commercial applications, such as good flexibility, wide working temperature, anti-freezing ability, and superior anti-self-discharging capability. Furthermore, standardizing tests and performance evaluation standard systems referring to devices should be carefully considered in practical applications.

In conclusion, developing ZHCs as appealing energy storage technology has significant opportunities and challenges. Tremendous efforts in electrode material studies are required to enhance the electrochemical performance of zinc-ion storage devices, accelerating the development of ZHCs in practical application. This review will provide valuable and constructive suggestions for carbon material studies to attract researchers to explore zinc-ion energy storage systems.

Conflicts of interest

The authors declare no conflict of interest.

Acknowledgements

References

1 D. Kundu, B. D. Adams, V. Duffort, S. H. Vajargah and L. F. Nazar, *Nat. Energy*, 2016, **1**, 1.
2 Y. Liang, W. H. Lai, Z. Miao and S. L. Chou, *Small*, 2018, **14**, 1702514.

This journal is © The Royal Society of Chemistry 2024

J. Mater. Chem. A, 2024, **12**, 9400–9420 | **9417**

3 Y. You and A. Manthiram, *Adv. Energy Mater.*, 2018, **8**, 1701785.

4 Y. Shao, M. F. El-Kady, J. Sun, Y. Li, Q. Zhang, M. Zhu, H. Wang, B. Dunn and R. B. Kaner, *Chem. Rev.*, 2018, **118**, 9233.

5 E. Olsson, J. Cottom, H. Au, Z. Guo, A. C. S. Jensen, H. Alptekin, A. J. Drew, M. M. Titirici and Q. Cai, *Adv. Funct. Mater.*, 2020, **30**, 1908209.

6 B. J. Landi, M. J. Ganter, C. D. Cress, R. A. DiLeo and R. P. Raffaelle, *Energy Environ. Sci.*, 2009, **2**, 638.

7 B. Yang, J. Chen, S. Lei, R. Guo, H. Li, S. Shi and X. Yan, *Adv. Energy Mater.*, 2018, **8**, 1702409.

8 B. K. Roy, I. Tahmid and T. U. Rashid, *J. Mater. Chem. A*, 2021, **9**, 17592.

9 J. Ding, W. Hu, E. Paek and D. Mitlin, *Chem. Rev.*, 2018, **118**, 6457.

10 J. Hao, X. Li, X. Zeng, D. Li, J. Mao and Z. Guo, *Energy Environ. Sci.*, 2020, **13**, 3917.

11 Z. Yao, V. I. Hegde, A. Aspuru-Guzik and C. Wolverton, *Adv. Energy Mater.*, 2019, **9**, 1802994.

12 X. Liu, Y. Sun, Y. Tong, X. Wang, J. Zheng, Y. Wu, H. Li, L. Niu and Y. Hou, *Nano Energy*, 2021, **86**, 106070.

13 Y. Xiong, Y. Lin and Q. Xue, *J. Electrochem. Soc.*, 2020, **167**, 160530.

14 Y. Liu, G. He, H. Jiang, I. P. Parkin, P. R. Shearing and D. J. L. Brett, *Adv. Funct. Mater.*, 2021, **31**, 2010445.

15 Q. Liu, H. Zhang, J. Xie, X. Liu and X. Lu, *Carbon Energy*, 2020, **2**, 521539.

16 Z. Wang, M. Zhang, W. Ma, J. Zhu and W. Song, *Small*, 2021, **17**, 2100219.

17 L. Dong, W. Yang, W. Yang, Y. Li, W. Wu and G. Wang, *J. Mater. Chem. A*, 2019, **7**, 13810.

18 A. Amiri, E. N. Swart and A. A. Polycarpou, *Renewable Sustainable Energy Rev.*, 2021, **148**, 111288.

19 H. Wang, W. Ye, Y. Yang, Y. Zhong and Y. Hu, *Nano Energy*, 2021, **85**, 105942.

20 M. Luo, X. Gan, C. Zhang, Y. Yang, W. Yue, I. Zhitomirsky and K. Shi, *Adv. Funct. Mater.*, 2023, **33**, 2305041.

21 X. Gan, J. Tang, X. Wang, L. Gong, I. Zhitomirsky, L. Qie and K. Shi, *Energy Storage Mater.*, 2023, **59**, 102769.

22 Y. Tian, R. Amal and D.-W. Wang, *Front. Energy Res.*, 2016, **4**, 34.

23 H. Wang, M. Wang and Y. Tang, *Energy Storage Mater.*, 2018, **13**, 1–7.

24 X. Li, M. Li, Q. Yang, H. Li, H. Xu, Z. Chai, K. Chen, Z. Liu, Z. Tang, L. Ma, Z. Huang, B. Dong, X. Yin, Q. Huang and C. Zhi, *ACS Nano*, 2020, **14**, 541.

25 G. H. An, J. Hong, S. Pak, Y. Cho, S. Lee, B. Hou and S. Cha, *Adv. Energy Mater.*, 2019, **10**, 1902981.

26 Z. Huang, A. Chen, F. Mo, G. Liang, X. Li, Q. Yang, Y. Guo, Z. Chen, Q. Li, B. Dong and C. Zhi, *Adv. Energy Mater.*, 2020, **10**, 2001024.

27 J. Zeng, L. Dong, L. Sun, W. Wang, Y. Zhou, L. Wei and X. Guo, *Nano-Micro Lett.*, 2020, **13**, 1.

28 S. Wang, Q. Wang, W. Zeng, M. Wang, L. Ruan and Y. Ma, *Nano-Micro Lett.*, 2019, **11**, 1.

29 L. Dong, W. Yang, W. Yang, C. Wang, Y. Li, C. Xu, S. Wan, F. He, F. Kang and G. Wang, *Nano-Micro Lett.*, 2019, **11**, 1.

30 Z. Huang, T. Wang, H. Song, X. Li, G. Liang, D. Wang, Q. Yang, Z. Chen, L. Ma, Z. Liu, B. Gao, J. Fan and C. Zhi, *Angew. Chem., Int. Ed.*, 2020, **60**, 1011.

31 Y. Sun, H. Ma, X. Zhang, B. Liu, L. Liu, X. Zhang, J. Feng, Q. Zhang, Y. Ding, B. Yang, L. Qu and X. Yan, *Adv. Funct. Mater.*, 2021, **31**, 2101277.

32 C. Wang, Z. Pei, Q. Meng, C. Zhang, X. Sui, Z. Yuan, S. Wang and Y. Chen, *Angew. Chem., Int. Ed.*, 2020, **60**, 990.

33 Z. Wang, J. Huang, Z. Guo, X. Dong, Y. Liu, Y. Wang and Y. Xia, *Joule*, 2019, **3**, 1289.

34 Q. Wu, L. Yang, X. Wang and Z. Hu, *Adv. Mater.*, 2019, **32**, 1904177.

35 T. Wu, J. Peng, W. Zhang, M. Zheng, J. Yang, Q. Lu, F. Xu, Y. Liu and Y. Liang, *Carbon Energy*, 2021, **3**, 554.

36 S. Roldán, C. Blanco, M. Granda, R. Menéndez and R. Santamaría, *Angew. Chem., Int. Ed.*, 2011, **50**, 1699.

37 A. Ponrouch, J. Bitenc, R. Dominko, N. Lindahl, P. Johansson and M. R. Palacin, *Energy Storage Mater.*, 2019, **20**, 253.

38 J. Huang, K. Yuan and Y. Chen, *Adv. Funct. Mater.*, 2022, **32**, 2108107.

39 N. Yang, S. Yu, W. Zhang, H. M. Cheng, P. Simon and X. Jiang, *Adv. Mater.*, 2022, **34**, 2202380.

40 S. Zhang and N. Pan, *Adv. Energy Mater.*, 2015, **5**, 1401401.

41 C.-C. Hu, K.-H. Chang, M.-C. Lin and Y.-T. Wu, *Nano Lett.*, 2006, **6**, 2690.

42 C. Xu, F. Kang, B. Li and H. Du, *J. Mater. Res.*, 2010, **25**, 1421.

43 D. P. Chatterjee and A. K. Nandi, *J. Mater. Chem. A*, 2021, **9**, 15880.

44 A. Patra, K. Namsheer, J. R. Jose, S. Sahoo, B. Chakraborty and C. S. Rout, *J. Mater. Chem. A*, 2021, **9**, 25852.

45 X. Gong, J. Chen and P. S. Lee, *Batteries Supercaps*, 2021, **4**, 1529.

46 L. Dong, X. Ma, Y. Li, L. Zhao, W. Liu, J. Cheng, C. Xu, B. Li, Q.-H. Yang and F. Kang, *Energy Storage Mater.*, 2018, **13**, 96.

47 X. Deng, J. Li, Z. Shan, J. Sha, L. Ma and N. Zhao, *J. Mater. Chem. A*, 2020, **8**, 11617.

48 Z. Li, D. Chen, Y. An, C. Chen, L. Wu, Z. Chen, Y. Sun and X. Zhang, *Energy Storage Mater.*, 2020, **28**, 307.

49 Y. Zhao, Y. Wang, Z. Zhao, J. Zhao, T. Xin, N. Wang and J. Liu, *Energy Storage Mater.*, 2020, **28**, 64.

50 J. Xiao, J. Han, C. Zhang, G. Ling, F. Kang and Q.-H. Yang, *Adv. Energy Mater.*, 2021, **12**, 2100775.

51 X. Wu, Y. Chen, Z. Xing, C. W. K. Lam, S. S. Pang, W. Zhang and Z. Ju, *Adv. Energy Mater.*, 2019, **9**, 1900343.

52 Q. Dou, N. Wu, H. Yuan, K. H. Shin, Y. Tang, D. Mitlin and H. S. Park, *Chem. Soc. Rev.*, 2021, **50**, 6734.

53 J. Li, L. Yu, Y. Li, G. Wang, L. Zhao, B. Peng, S. Zeng, L. Shi and G. Zhang, *Nanoscale*, 2021, **13**, 692.

54 Z. Heidarinejad, M. H. Dehghani, M. Heidari, G. Javedan, I. Ali and M. Sillanpää, *Environ. Chem. Lett.*, 2020, **18**, 393.

55 Z. Xu, M. Wu, Z. Chen, C. Chen, J. Yang, T. Feng, E. Paek and D. Mitlin, *Adv. Sci.*, 2019, **6**, 1802272.

9418 | *J. Mater. Chem. A*, 2024, **12**, 9400–9420

This journal is © The Royal Society of Chemistry 2024

56 S. Zhang, M. Zheng, Y. Tang, R. Zang, X. Zhang, X. Huang, Y. Chen, Y. Yamauchi, S. Kaskel and H. Pan, *Adv. Funct. Mater.*, 2022, **32**, 2204714.

57 Z. Zhou, X. Zhou, M. Zhang, S. Mu, Q. Liu and Y. Tang, *Small*, 2020, **16**, 2003174.

58 G.-H. An, *Appl. Surf. Sci.*, 2020, **530**, 147220.

59 C. Wang, X. Zeng, P. J. Cullen and Z. Pei, *J. Mater. Chem. A*, 2021, **9**, 19054.

60 L. Han, H. Huang, X. Fu, J. Li, Z. Yang, X. Liu, L. Pan and M. Xu, *Chem. Eng. J.*, 2020, **392**, 123733.

61 P. Zhang, Y. Li, G. Wang, F. Wang, S. Yang, F. Zhu, X. Zhuang, O. G. Schmidt and X. Feng, *Adv. Mater.*, 2019, **31**, 1806005.

62 J. Wang, P. Nie, B. Ding, S. Dong, X. Hao, H. Dou and X. Zhang, *J. Mater. Chem. A*, 2017, **5**, 2411.

63 M. S. Javed, T. Najam, I. Hussain, M. Idrees, A. Ahmad, M. Imran, S. S. A. Shah, R. Luque and W. Han, *Adv. Energy Mater.*, 2023, **13**, 2202303.

64 L. He, Y. Liu, C. Li, D. Yang, W. Wang, W. Yan, W. Zhou, Z. Wu, L. Wang, Q. Huang, Y. Zhu, Y. Chen, L. Fu, X. Hou and Y. Wu, *ACS Appl. Energy Mater.*, 2019, **2**, 5835.

65 G. Yang, J. Huang, X. Wan, Y. Zhu, B. Liu, J. Wang, P. Hiralal, O. Fontaine, Y. Guo and H. Zhou, *Nano Energy*, 2021, **90**, 106500.

66 Y. Ruquan and J. M. Tour, *ACS Nano*, 2019, **13**, 10872.

67 H. Huang, H. Shi, P. Das, J. Qin, Y. Li, X. Wang, F. Su, P. Wen, S. Li, P. Lu, F. Liu, Y. Li, Y. Zhang, Y. Wang, Z.-S. Wu and H.-M. Cheng, *Adv. Funct. Mater.*, 2020, **30**, 1909035.

68 L. Zhang, D. Wu, G. Wang, Y. Xu, H. Li and X. Yan, *Chin. Chem. Lett.*, 2021, **32**, 926.

69 Y. Zhu, X. Ye, H. Jiang, J. Xia, Z. Yue, L. Wang, Z. Wan, C. Jia and X. Yao, *J. Power Sources*, 2020, **453**, 227851.

70 S. Wu, Y. Chen, T. Jiao, J. Zhou, J. Cheng, B. Liu, S. Yang, K. Zhang and W. Zhang, *Adv. Energy Mater.*, 2019, **9**, 1902915.

71 G. Sun, Y. Xiao, B. Lu, X. Jin, H. Yang, C. Dai, X. Zhang, Y. Zhao and L. Qu, *ACS Appl. Mater. Interfaces*, 2020, **12**, 7239.

72 Y. Shao, Z. Sun, Z. Tian, S. Li, G. Wu, M. Wang, X. Tong, F. Shen, Z. Xia, V. Tung, J. Sun and Y. Shao, *Adv. Funct. Mater.*, 2020, **31**, 2007843.

73 Y. Xu, X. Chen, C. Huang, Y. Zhou, B. Fan, Y. Li, A. Hu, Q. Tang and K. Huang, *J. Power Sources*, 2021, **488**, 229426.

74 P. Pattananuwat, R. Pornprasertsuk, J. Qin and S. Prasertkaewf, *RSC Adv.*, 2021, **11**, 35205.

75 F.-Z. Cui, Z. Liu, D.-L. Ma, L. Liu, T. Huang, P. Zhang, D. Tan, F. Wang, G.-F. Jiang and Y. Wu, *Chem. Eng. J.*, 2021, **405**, 127038.

76 J. Yang, J. Cao, Y. Peng, M. Bissett, I. A. Kinloch and R. A. W. Dryfe, *J. Power Sources*, 2021, **516**, 230663.

77 W. Tian, H. Zhang, X. Duan, H. Sun, G. Shao and S. Wang, *Adv. Funct. Mater.*, 2020, **30**, 1909265.

78 J. Kim, M. S. Choi, K. H. Shin, M. Kota, Y. Kang, S. Lee, J. Y. Lee and H. S. Park, *Adv. Mater.*, 2019, **31**, 1803444.

79 D. K. Sam, H. Li, Y. Xu and Y. Cao, *J. Ind. Eng. Chem.*, 2024, DOI: 10.1016/j.jiec.2024.01.044.

80 S. Chen, L. Ma, K. Zhang, M. Kamruzzaman, C. Zhi and J. A. Zapien, *J. Mater. Chem. A*, 2019, **7**, 7784.

81 Y. Zhang, Z. Wang, D. Li, Q. Sun, K. Lai, K. Li, Q. Yuan, X. Liu and L. Ci, *J. Mater. Chem. A*, 2020, **8**, 22874.

82 P. Liu, W. Liu, Y. Huang, P. Li, J. Yan and K. Liu, *Energy Storage Mater.*, 2020, **25**, 858.

83 R. Fei, H. Wang, Q. Wang, R. Qiu, S. Tang, R. Wang, B. He, Y. Gong and H. J. Fan, *Adv. Energy Mater.*, 2020, **10**, 2002741.

84 J. Yin, W. Zhang, N. A. Alhebshi, N. Salah and H. N. Alshareef, *Small Methods*, 2020, **4**, 1900853.

85 H. Li, J. Wu, L. Wang, Q. Liao, X. Niu, D. Zhang and K. Wang, *Chem. Eng. J.*, 2022, **428**, 131071.

86 X. Fan, P. Liu, B. Ouyang, R. Cai, X. Chen, X. Liu, W. Liu, J. Wang and K. Liu, *ChemElectroChem*, 2021, **8**, 3572.

87 Z. Pan, Z. Lu, L. Xu and D. Wang, *Appl. Surf. Sci.*, 2020, **510**, 145384.

88 Z. Bi, Q. Kong, Y. Cao, G. Sun, F. Su, X. Wei, X. Li, A. Ahmad, L. Xie and C.-M. Chen, *J. Mater. Chem. A*, 2019, **7**, 16028.

89 P. Yu, P. Zeng, Y. Zeng, H. Dong, H. Hu, Y. Liu, M. Zheng, Y. Xiao, X. Lu and Y. Liang, *Electrochim. Acta*, 2019, **327**, 134999.

90 J. Yin, W. Zhang, W. Wang, N. A. Alhebshi, N. Salah and H. N. Alshareef, *Adv. Energy Mater.*, 2020, **10**, 2001705.

91 L. Wang, M. Huang, J. Huang, X. Tang, L. Li, M. Peng, K. Zhang, T. Hu, K. Yuan and Y. Chen, *J. Mater. Chem. A*, 2021, **9**, 15404.

92 H. He, J. Lian, C. Chen, Q. Xiong and M. Zhang, *Chem. Eng. J.*, 2021, **421**, 129786.

93 X. Feng, Y. Bai, M. Liu, Y. Li, H. Yang, X. Wang and C. Wu, *Energy Environ. Sci.*, 2021, **14**, 2036.

94 W. Chen, M. Wan, Q. Liu, X. Xiong, F. Yu and Y. Huang, *Small Methods*, 2018, **3**, 1800323.

95 Y. Yuan, Z. Chen, H. Yu, X. Zhang, T. Liu, M. Xia, R. Zheng, M. Shui and J. Shu, *Energy Storage Mater.*, 2020, **32**, 65.

96 D. Wang, Z. Pan, G. Chen and Z. Lu, *Electrochim. Acta*, 2021, **379**, 138170.

97 H. Zhang, Q. Liu, Y. Fang, C. Teng, X. Liu, P. Fang, Y. Tong and X. Lu, *Adv. Mater.*, 2019, **31**, 1904948.

98 P. Liu, Y. Gao, Y. Tan, W. Liu, Y. Huang, J. Yan and K. Liu, *Nano Res.*, 2019, **12**, 2835.

99 J. Huang, L. Wang, Z. Peng, M. Peng, L. Li, X. Tang, Y. Xu, L. Tan, K. Yuan and Y. Chen, *J. Mater. Chem. A*, 2021, **9**, 8435.

100 D. Wang, S. Wang and Z. Lu, *Int. J. Energy Res.*, 2021, **45**, 2498.

101 X. Shi, H. Zhang, S. Zeng, J. Wang, X. Cao, X. Liu and X. Lu, *ACS Mater. Lett.*, 2021, **3**, 1291.

102 Y. Li, W. Yang, W. Yang, Z. Wang, J. Rong, G. Wang, C. Xu, F. Kang and L. Dong, *Nano-Micro Lett.*, 2021, **13**, 95.

103 W. Feng, N. Feng, W. Liu, Y. Cui, C. Chen, T. Dong, S. Liu, W. Deng, H. Wang and Y. Jin, *Adv. Energy Mater.*, 2020, **11**, 2003215.

104 C.-C. Hou, Y. Wang, L. Zou, M. Wang, H. Liu, Z. Liu, H. F. Wang, C. Li and Q. Xu, *Adv. Mater.*, 2021, **33**, 2101698.

105 J. Li, J. Zhang, L. Yu, J. Gao, X. He, H. Liu, Y. Guo and G. Zhang, *Energy Storage Mater.*, 2021, **42**, 705.

This journal is © The Royal Society of Chemistry 2024

J. Mater. Chem. A, 2024, **12**, 9400–9420 | **9419**

106 H. Fan, X. Hu, S. Zhang, Z. Xu, G. Gao, Y. Zheng, G. Hu, Q. Chen, T. S. AlGarni and R. Luque, *Carbon*, 2021, **180**, 254.

107 H. Zhang, Z. Chen, Y. Zhang, Z. Ma, Y. Zhang, L. Bai and L. Sun, *J. Mater. Chem. A*, 2021, **9**, 16565.

108 Y. Lu, Z. Li, Z. Bai, H. Mi, C. Ji, H. Pang, C. Yu and J. Qiu, *Nano Energy*, 2019, **66**, 104132.

109 L. Han, X. Zhang, J. Li, H. Huang, X. Xu, X. Liu, Z. Yang, M. Xu and L. Pan, *J. Colloid Interface Sci.*, 2021, **599**, 556.

110 L. Huang, Y. Xiang, M. Luo, Q. Zhang, H. Zhu, K. Shi and S. Zhu, *Carbon*, 2021, **185**, 1.

111 G. Fang, J. Zhou, A. Pan and S. Liang, *ACS Energy Lett.*, 2018, **3**, 2480.

112 C. Wang, Z. Pei, Q. Meng, C. Zhang, X. Sui, Z. Yuan, S. Wang and Y. Chen, *Angew. Chem., Int. Ed.*, 2020, **60**, 990.

113 Y. Sun, B. Liu, L. Liu, J. Lang and J. Qiu, *Small Struct.*, 2023, **4**, 2200345.

114 J. Li, L. Yu, W. Wang, X. He, G. Wang, R. Liu, X. Ma and G. Zhang, *J. Mater. Chem. A*, 2022, **10**, 9355.

115 Z. Tie and Z. Niu, *Angew. Chem., Int. Ed.*, 2020, **59**, 21293.

116 X. Qiu, N. Wang, Z. Wang, F. Wang and Y. Wang, *Angew. Chem., Int. Ed.*, 2021, **60**, 9610.

117 X. Gan, C. Zhang, X. Ye, L. Qie and K. Shi, *Energy Storage Mater.*, 2024, **65**, 103175.

118 L. Zhang, G. Wang, J. Feng, Q. Ma, Z. Liu and X. Yan, *ChemElectroChem*, 2021, **8**, 1289.

119 L. Wan, H. Zhang, M. Qu, M. Feng, Z. Shang, R. Wang, D. Lei and Y. Cui, *Energy Storage Mater.*, 2023, **63**, 102982.

120 K. A. Owusu, X. Pan, R. Yu, L. Qu, Z. Liu, Z. Wang, M. Tahir, W. A. Haider, L. Zhou and L. Mai, *Mater. Today Energy*, 2020, **18**, 100529.

121 K. Zou, P. Cai, X. Deng, B. Wang, C. Liu, Z. Luo, X. Lou, H. Hou, G. Zou and X. Ji, *Chem. Commun.*, 2021, **57**, 528.

122 D. Han, S. Wu, S. Zhang, Y. Deng, C. Cui, L. Zhang, Y. Long, H. Li, Y. Tao, Z. Weng, Q. H. Yang and F. Kang, *Small*, 2020, **16**, 2001736.

123 W. Fan, J. Ding, J. Ding, Y. Zheng, W. Song, J. Lin, C. Xiao, C. Zhong, H. Wang and W. Hu, *Nano-Micro Lett.*, 2021, **13**, 1.

9420 | *J. Mater. Chem. A*, 2024, **12**, 9400–9420

This journal is © The Royal Society of Chemistry 2024